Hindawi
Journal of Chemistry
Volume 2019, Article ID 6728492, 20 pages
https://doi.org/10.1155/2019/6728492

Research Article

Analysis of CaF_2 Precipitation Process in the Selected Static Mixers

Piotr Maria Synowiec and Magdalena Stec

Department of Chemical Engineering and Process Design, Faculty of Chemistry, Silesian University of Technology, Strzody 7, 44-100 Gliwice, Poland

Correspondence should be addressed to Magdalena Stec; magdalena.stec@polsl.pl

Received 19 October 2018; Revised 5 December 2018; Accepted 24 December 2018; Published 11 February 2019

Academic Editor: José L. Arias Mediano

In the paper, the analysis of the precipitation process of calcium fluoride in the selected static mixers was made. The Kenics and Koflo static mixers, as well as an empty pipe as a background, have been taken into consideration. The Kenics and Koflo types have been chosen as their inner shapes convenient for the realization of continuous precipitation processes as incrustation phenomenon and dangerousness of flow blocking are not as high as in other solutions. The main tasks were focused on the recognition of the precipitation kinetics (to get the knowledge of the relative supersaturation, nucleation sources, and mechanisms controlling the crystal growth), determination of conversion efficiency of the chemical reaction by which CaF_2 is precipitated, the fluid dynamic conditions on crystal size distribution (CSD), and the identification of particles' destruction sources as well. This paper is a *primary* work dedicated to the possibilities of a special treatment of the solid phase during its formation in order to obtain the required crystal size distribution (CSD) and to avoid the agglomeration when necessary. The results are very promising. As it will be shown, the special treatment of the precipitated solid substances in static mixers enables to create crystals with the required size and to eliminate the agglomeration phenomenon.

1. Introduction

The CSD (crystal size distribution) strongly depends on fluid dynamic conditions especially in chemical reactors with static inserts. The main cause of differences in the mean crystal sizes is connected with the supersaturation of solution, the residence time distribution and, at last but not at least, with the various destruction sources, in which values depend precisely on the fluid dynamics. That is why, to conduct the crystallization processes, it is so important to prepare the complete fluid dynamic characteristics of the devices considered to this process and to get knowledge of the possible ways of destruction.

In the case of sparingly soluble substances, crystallization by evaporation or cooling is not efficient, that is why the crystallization with chemical reaction should be used. In comparison to the first mentioned method, the relative supersaturation obtained in precipitation processes is much higher and, in consequence, the crystal size of the final product is usually smaller.

The presented paper takes into account the analysis of the CaF_2 precipitation process by means of $Ca(NO_3)_2$ and NH_4F solutions, which in contrast to other researchers provided in stirred tanks [1–4] or reactor with the fluidized bed [5] was carried out in two types of static mixers: Kenics and Koflo, and empty pipe treated as comparison background. The selection of the mentioned mixers' geometries was dictated by the favorable construction of static inserts that are resistant to crystals' deposits. The shape of static inserts for both mixer types is presented in Figures 1(a) and 1(b).

The choice of static mixers use in crystallization processes, instead of vessels with mechanical agitators, was connected with high mixing efficiency and more uniform unit power input distribution which plays a key role in the considered process as it eliminates the potential existence of regions with uncontrolled supersaturation [6]. The relatively short residence time in static mixers, in the case of fast ionic reactions, does not play a negative role. What is more, there is a very limited number of publications, [6–10] that consider the use of mixers

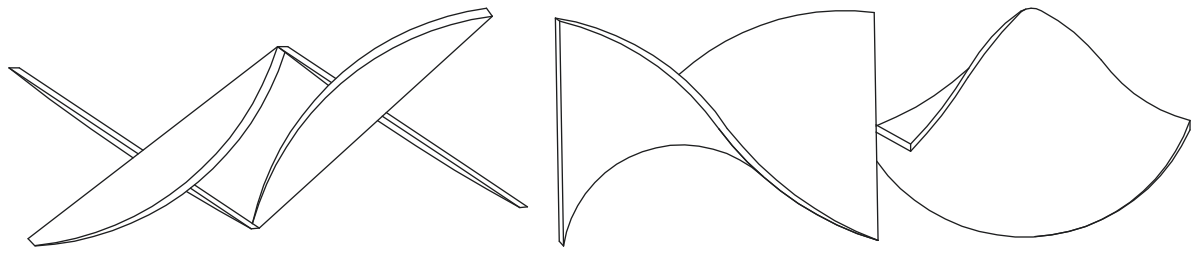

Figure 1: The shape of mixers' inserts: (a) Koflo static mixer; (b) Kenics static mixer.

with static inserts in reaction crystallization in a very similar way.

In the main part of the study, the authors tried to find the answer on the following issues:

(i) The value of the relative supersaturation
(ii) The nucleation sources
(iii) The mechanism limiting the crystal growth
(iv) The conversion rate of the chemical reaction by which CaF_2 is precipitated
(v) The relation between fluid dynamic conditions and crystal size distribution
(vi) The crystals' destruction sources
(vii) The physical model describing the relation between the particle size and the fluid dynamic conditions of flow

Especially fourth and fifth terms are very important for industrial practice as conversion efficiency affects the fluorites corrosion rate reduction and CSD influences on CaF_2 separation effectiveness in the centrifuge from the stream of ammonium sulfate solution.

2. The Origin of the Research

Initialization of the research was connected with the previous investigations focused on the fluid dynamic analysis [11–13]. During the investigations related to the recognition of flow conditions in the selected static mixers like Koflo and Kenics, it was found that the value of the CoV coefficient, the parameter describing a mixture homogeneity (defined as the ratio of the standard deviation and the mean concentration—equation (1)) is almost similar to that in the pipe for the Reynolds number higher than 2000. In the range of smaller values of Re, a big difference between CoV values was found (Figure 2):

$$\mathrm{CoV} = \frac{S'}{\overline{C}} \cdot 100 = \frac{\sqrt{\sum_{i=1}^{n} (C_i - \overline{C})^2 / n - 1}}{\sum_{i=1}^{n} C_i} \cdot 100 \ (\%). \quad (1)$$

In most of the practical applications, the CoV value less than 5% is fully satisfying [15]. As observed from Figure 2, this condition is fulfilled in static mixers in the whole analyzed range of the Reynolds numbers. However, for the empty pipe, CoV < 5% may be reached for Re number higher than 1000.

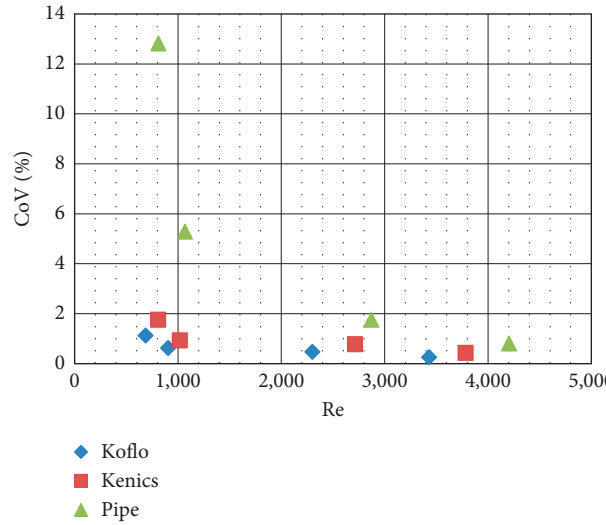

Figure 2: CoV versus Re number for considered devices [14].

Unfortunately, a huge pressure drop in comparison to an empty pipe (Figure 3) occupies those favorable CoV values in the mentioned static mixers.

Taking into consideration the presented observations, a dilemma was arising—when, in the practical application, is necessary to use a static mixer in precipitation processes and when an empty pipe may be used.

3. Theory

3.1. The Driving Force of the Crystallization Process. To carry out the crystallization process, it is required to induce the supersaturation in a solution. The definition of supersaturation Δc says that it is a difference between the actual concentration c and the concentration of the saturated solution (in other words, the solubility c^*).

In practice, more common is a concept of the relative supersaturation σ, which, in turn, may be presented as follows:

$$\sigma = \frac{\Delta c}{c^*} \ (-). \quad (2)$$

In the literature [4, 16–18], more versatile form of the equation for σ is used (equation (3)). It was proposed by Nielsen and Toft [19], and it is suitable for sparingly soluble salts (like the considered CaF_2):

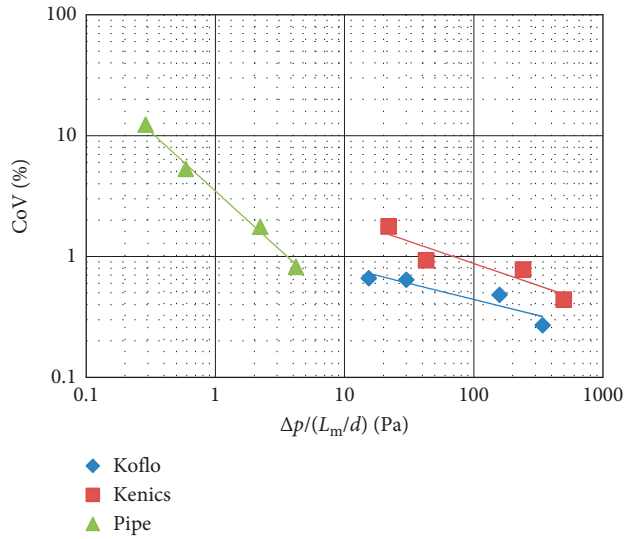

Figure 3: CoV versus unit pressure drop [14].

$$\sigma = \left(\frac{\mathrm{IP}}{K_{\mathrm{sp}}}\right)^{1/\nu} - 1 \ (-). \tag{3}$$

In the presented formula (equation (3)), IP is the ionic product of activity, K_{sp} is the solubility product, and ν is the sum of stoichiometric coefficients of reactants.

For such a salt dissociation, the following equation is presented:

$$A_x B_y \longleftrightarrow xA^{z-} + yB^{z+}, \tag{4}$$

and the ionic product of activity IP may be calculated on the basis of the following equation:

$$\mathrm{IP} = (a_A)^x \cdot (a_B)^y = (c_A \cdot \gamma_A)^x \cdot (c_B \cdot \gamma_B)^y, \tag{5}$$

where γ is the ion activity coefficient, dependent on the value of ionic strength I (equation (6)), which may be determined on the basis of one from the following formulas (equations (7)–(9)):

$$I = \frac{1}{2}\sum_{i=1}^{n} z_i^2 \cdot c_i \ \left(\mathrm{kmol/m^3}\right). \tag{6}$$

(i) For $I < 0.01$ from the Debye–Hückel theory,

$$\log \gamma_i = -A' \cdot z_i^2 \cdot \sqrt{I}. \tag{7}$$

(ii) For $I < 0.1$ from the extended Debye–Hückel theory which takes into account the influence of ion radii d_i on the activity coefficient,

$$\log \gamma_i = -\frac{A' \cdot z_i^2 \cdot \sqrt{I}}{1 + B' \cdot d_i \cdot \sqrt{I}}. \tag{8}$$

(iii) For $I < 0.5$ from the Davies equation,

$$\log \gamma_i = -A' \cdot z_i^2 \cdot \left(\frac{\sqrt{I}}{1+\sqrt{I}} - 0.3I\right), \tag{9}$$

where A' and B' are constants; in aqueous solution at 25°C, $A' = 0.51$ and $B' = 3.3 \cdot 10^7$.

3.2. The Nucleation Sources. The crystallization process is inseparably linked with two processes: nucleation and crystal growth. Nucleation is the creation of crystals nuclei in the supersaturated solution which then grows to reach the size of crystals. Depending on the solution supersaturation, primary and secondary nucleation is distinguished [2, 20].

3.3. The Crystal Growth Mechanism. In accordance with the literature [21], it may be written that crystal growth rate may be controlled through the following:

(i) Heat transfer

(ii) Bulk diffusion

(iii) Surface integration

In the case of melt crystallization, heat transfer is the controlling step because the two other mechanisms are much faster. The situation is different when the crystallization from solution is taken into account. There the control mechanism depends on the supersaturation value. If the operating supersaturation is high (or even super high), the crystal growth rate is controlled by bulk diffusion and depends on the mass transfer coefficient. If the supersaturation is low, then the surface integration plays a key role in the crystal growth. In practice, such definitions are not very precise because there is no direct line which would divide supersaturation into high and low. To unambiguously state which mechanism is a limiting one, the conditions presented in equations (10) and (11) should be checked [21]:

(i) The bulk diffusion is as a controlling step when the relative supersaturation σ excesses the value:

$$\sigma > 0.01 \cdot \sqrt{\frac{c_{\mathrm{c}}}{c^*}}. \tag{10}$$

(ii) In turn, for the values of relative supersaturation less than the multiplication result in equation (11), the surface integration starts to play a more important role and "controls" the crystal growth:

$$\sigma < 2 \cdot 10^{-4} \cdot \sqrt{\frac{c_{\mathrm{c}}}{c^*}}, \tag{11}$$

where

$$c_{\mathrm{c}} = \frac{\rho}{M}\left(\mathrm{kmol/m^3}\right), \tag{12}$$

$$c^* = \sqrt[3]{K_{\mathrm{sp}}}\left(\mathrm{kmol/m^3}\right). \tag{13}$$

3.4. Identification of the Crystals' Potential Destruction Sources. During each mass crystallization process, the final product size depends on the crystal physical growth rate and agglomeration as well and the opposite-directed crystal destruction.

Because of the fact that the microscopic observations (by the use of a SEM technique) of the obtained solid particles showed no evidence of agglomerates existence, the

agglomeration, as a phenomenon that may affect the final crystals size, was neglected. Such a state of affairs was also checked and confirmed by the measurements of the crystal density, carried out by the use of the gas displacement pycnometry device. The obtained values were similar to the physical one for the homogeneous CaF_2 crystal.

The sources of destruction may have different bases. In our opinion, in the case of static mixers used as crystallizers, the potential destruction of particles (and the source of a secondary nucleation) may be mainly generated by means of the following:

(i) Crystal-crystal mechanical collisions

(ii) Crystal-static inserts mechanical collisions

(iii) Shear stresses tangent to the crystal's surface and caused by the relative velocity u_r of a particle to the surrounding solution

The collisions between particles and the inner mixer's wall have not been taken into consideration as relatively small in comparison to other sources [22, 23].

In order to analyze the influence of flow conditions on CSD, the particular unit destruction energy e_{des} (J/kg) for different destruction sources should be calculated according to the following equations (equations (14)–(21)).

(i) Mechanical collisions may be described as follows:

(a) Crystal-crystal collisions:

$$e_{\mathrm{coll}_{c-c}} = \frac{E_{\mathrm{coll}_{c-c}}}{m_c}\,(\mathrm{J/kg}), \tag{14}$$

$$E_{\mathrm{coll}_{c-c}} = \frac{1}{2}\cdot k_v \cdot L_{\mathrm{mean}}^3 \cdot \rho_c \cdot u_r^2\,(\mathrm{J}), \tag{15}$$

where the relative velocity is defined as [24]

$$u_r = \left(\frac{\Delta\rho}{\rho}\right)\cdot\left(\frac{\rho_c}{\rho}\right)\cdot \varepsilon^{1/3}\cdot\left(\frac{1}{c_{DC}}\right)^{1/3}\cdot L_{\mathrm{mean}}^{1/3}\,(\mathrm{m/s}). \tag{16}$$

(b) Crystal-static inserts collisions (present only in static mixers) may be described as follows:

$$e_{\mathrm{coll}_{c-si}} = \frac{E_{\mathrm{coll}_{c-si}}}{m_c}\,(\mathrm{J/kg}), \tag{17}$$

$$E_{\mathrm{coll}_{c-si}} = \frac{1}{2}\cdot k_v \cdot L_{\mathrm{mean}}^3 \cdot \rho_c \cdot w^2 \cdot \sin\alpha\,(\mathrm{J}), \tag{18}$$

where the particle velocity w was assumed as equal to the liquid velocity.

(i) Maximum shear stresses were estimated as follows:

$$e_{\mathrm{shear}} = \frac{E_{\mathrm{shear}}}{m_c}\,(\mathrm{J/kg}), \tag{19}$$

$$E_{\mathrm{shear}} = V_c \cdot \tau_s\,(\mathrm{J}), \tag{20}$$

where

$$\tau_s = \frac{1}{2}\cdot \rho \cdot w^2 \cdot c_{DC}\,(\mathrm{Pa}). \tag{21}$$

However, for a more precise description of a destruction phenomenon, also the frequency of attrition source and the duration time should be taken into consideration. That is why the authors propose to calculate the effective destruction energy e_{eff} (equation (22)), which takes into account not only the value of the total energy destruction e_{total} but also the frequency of interactions f_i as well as the mean residence time t_m (detailed explanation about the determination of t_m may be found in [12]).

That finally gives

$$e_{\mathrm{eff}_i} = e_i \cdot f_i \cdot t_m\,(\mathrm{J/kg}), \tag{22}$$

where e_i means, respectively, the unit mechanical energy of crystal-crystal collisions (c-c) or the mechanical energy of crystal-inserts collisions (c-si) or the shear energy (shear).

The frequency of interaction f_i may be determined by the use of following relations:

(i) Crystal-static inserts:

$$f_{c-si} = \frac{\dot{V}}{V_{si}}\,(1/\mathrm{s}). \tag{23}$$

(ii) Crystal-crystal [23]:

$$f_{c-c} = n_c \cdot k_f \cdot L_{\mathrm{mean}}^2 \cdot u_r\,(1/\mathrm{s}). \tag{24}$$

(iii) Shear stresses:

$$f_{\mathrm{shear}} = 1\,(1/\mathrm{s}), \tag{25}$$

where V_{si} is the elemental volume within one static insert (equation (26)):

$$V_{si} = h \cdot F\left(\mathrm{m}^3\right), \tag{26}$$

and n_c is the number of crystals per unit volume (equation (27)):

$$n_c = \frac{\phi}{k_v \cdot L_{\mathrm{mean}}^3}\left(1/\mathrm{m}^3\right). \tag{27}$$

In the case of shear stresses, the frequency of interaction f_{shear} is assumed to be equal to 1 because during the fluid motion, they are continuously generated on crystal's surfaces. Admittedly, the velocity w used for the unit shear energy e_{shear} estimation gives the maximum possible value.

In turn, the total unit destruction energy e_{total}, that may be used for the recognition of the main destruction, will be the sum of the particular unit energies e_{eff_i} (equations (28) and (29)):

(i) Static mixers:

$$e_{\mathrm{totalSM}} = e_{\mathrm{eff}_{c-c}} + e_{\mathrm{eff}_{c-si}} + e_{\mathrm{eff}_{\mathrm{shear}}}\,(\mathrm{J/kg}). \tag{28}$$

(ii) Pipe:

$$e_{\mathrm{totalpipe}} = e_{\mathrm{eff}_{c-c}} + e_{\mathrm{eff}_{\mathrm{shear}}}\,(\mathrm{J/kg}). \tag{29}$$

As will be shown in the next pages, the shear stresses do not play an important role in the destruction of crystals. For that reason, it will not be taken into account during the further considerations.

4. Experimental

The presented study took into account the precipitation of CaF_2 from NH_4F solution, by means of $Ca(NO_3)_2$, in stoichiometric proportions:

$$2NH_4F + Ca(NO_3)_2 \longrightarrow CaF_2\downarrow + 2NH_4NO_3 \quad (30)$$

Both laminar and turbulent flow regimes were investigated (as mentioned earlier, the examined Reynolds numbers were in the range of 600–3500) in two types of static mixers (differing from each other in the shape of motionless inserts) as well as in an empty pipe, used as a background. The investigated relative supersaturation σ, calculated in accordance with the relevant literature [4, 16–18] on the basis of the ionic product of activity IP and the solubility product K_{sp}, was equal to 157. The dimensions of the tested devices and the properties of used reactants are showed in Tables 1 and 2, respectively.

The experiments were carried out in the laboratory setup presented in Figure 4.

The substrates 0.244 M water solution of ammonium fluoride (NH_4F) and 0.122 M water solution of calcium nitrate ($Ca(NO_3)_2$) were collected in the feed tanks (1).

The concentrations of solutions have been selected in such a way as to ensure the stoichiometric proportions of the reactants during the flow through the device (static mixers/pipe). To enable the postprocessing calculations connected with the preparation of population balances and calculations of fluorides removal conversion rates, some measurements in the feed tanks were made. In both substrates solutions, density (by the use of densimeter Anton Paar with the accuracy $\pm 5 \cdot 10^{-5}$ g/cm^3), viscosity (viscometer ViscoLab400, precision ±1.5%), and pH value (pH meter Elmetron CP-401, precision class ± 0.002 pH) were specified. What is more, in NH_4F solution, the initial concentration of fluoride ions was determined by the use of ion meter (Elmetron CPI-505, accuracy ±0.25%) equipped with the fluoride ion selective electrode (IJ-F IONODE, measuring range 0.02–19000 ppm). The measurements were carried by the use of TISAB buffer solution in order to mask minor changes of the ionic strength and to increase the accuracy of the reading.

From the feed tanks (1), the solutions in equal amounts (each in the separate pipeline) were pumped by metering pumps (with the automatic adjustment of the revolution number, accuracy ±0.05%) (2) to the static mixer/pipe (3). The liquid-solid suspension, obtained as a result of chemical reaction between substrates, was taken to analyse by the use of a nozzle (6) placed downstream the mixer. The rest of the suspension was directed to the storage tank (4) and next for disposal.

The obtained reaction product, in the form of crystals, was subjected to vacuum filtration, washing (by the use of 99.8% ethanol, analytical standard) and drying at the temperature of 60°C. Then, it was directed to other analyses such as SEM observations (scanning electron microscope Hitachi TM 3000) and laser particle size analyses (Fritsch Analysette 22, measuring range 1000–0.1 μm) to get the knowledge of crystals' shape and CSD.

In the mother liquor, the concentration of fluorides and pH value was measured by the use of mentioned earlier equipment.

The experimental setup was also equipped with additional temperature sensors (precision ±0.1°C) and thermostats (accuracy ±0.03°C) (7), as well as control valves (5), that enable the permanent control of the processing media.

Table 1: Dimensions of the tested devices.

	Koflo	Kenics	Pipe
Number of mixing elements	6	6	—
Inner diameter (m)	0.015	0.0136	0.015
Device length (m)	0.186	0.165	0.186
Thickness of mixing elements (m)	0.0017	0.004	—
	12.40	12.13	12.40
Length/diameter	18.67	—	18.67
	31.07	—	31.07
Device active volume for			
$L_m/d = 12.4$	16.4	14.5	32.8
$L_m/d = 18.67$	24.7	—	49.5
$L_m/d = 31.07$ (mL = 10^{-6} m^3)	41.0	—	82.3

Table 2: Properties of the substrates.

Property	Component	
	NH_4F_{aq}	$Ca(NO_3)_{2\ aq}$
Density, ρ (kg/m^3) ($t^* = 20$°C)	1003	1013.7
pH	6.949	7.269
Viscosity, η' (Pa·s) ($t^* = 20$°C)	$1 \cdot 10^{-3}$	$1 \cdot 10^{-3}$

5. Results and Discussion

5.1. Determination of the Relative Supersaturation. According to the information presented in the theory section, the calculation aimed at the supersaturation determination σ was made. All equations referring to the considered CaF_2 precipitation case are presented (equations (31)–(35)). The obtained results are collected in Table 3:

$$CaF_2\downarrow \longrightarrow Ca^{2+} + 2F^-$$

$$IP = (a_{Ca^{2+}})^1 \cdot (a_{F^-})^2 = (c_{Ca^{2+}} \cdot \gamma_{Ca^{2+}})^1 \cdot (c_{F^-} \cdot \gamma_{F^-})^2, \quad (31)$$

$$I = \frac{1}{2}\left(z_{Ca^{2+}} \cdot c_{Ca^{2+}} + z^2_{F^-} \cdot c_{F^-} + z^2_{NH_4^+} \cdot c_{NH_4^+} + z^2_{NO_3^-} \cdot c_{NO_3^-}\right). \quad (32)$$

Because of the fact that the calculated value of the solution ionic strength $I = 0.305$ (kmol/m^3), the activity

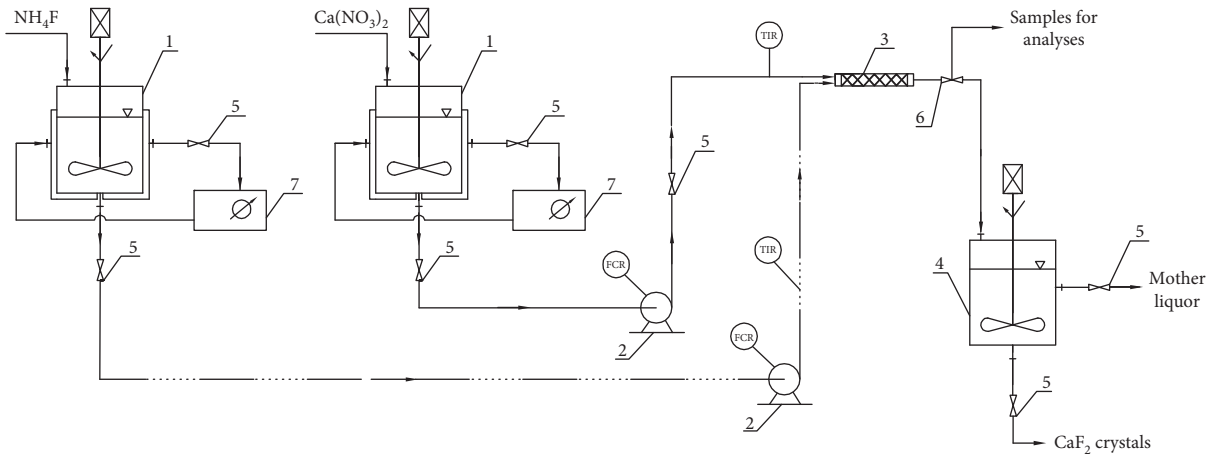

Figure 4: Experimental setup. 1, feed tank with a stirrer; 2, metering pump; 3, static mixer/pipe; 4, storage tank; 5, control valve; 6, sampling nozzle; 7, thermostat. Equipment instrumentation and automatics: flow rate automatic adjustment with registration (FCR) and temperature measurement with the identification of a setpoint value and registration (TIR).

Table 3: Calculation results.

Calculated parameter	Value
Ionic product of activity $((\text{kmol/m}^3)^3)$	$1.41 \cdot 10^{-4}$
Activity coefficient of F^- γ_{F^-}	0.733
Activity coefficient of Ca^{2+} $\gamma_{Ca^{2+}}$	0.289
Relative supersaturation σ	157

coefficients were calculated on the basis of the Davies equation (equation (9)):

$$\log \gamma_{Ca^{2+}} = -0.51 \cdot \left(z_{Ca^{2+}}\right)^2 \cdot \left(\frac{\sqrt{I}}{1+\sqrt{I}} - 0.3I\right), \quad (33)$$

$$\log \gamma_{F^-} = -0.51 \cdot \left(z_{F^-}\right)^2 \cdot \left(\frac{\sqrt{I}}{1+\sqrt{I}} - 0.3I\right), \quad (34)$$

$$\sigma = \left(\frac{\text{IP}}{K_{sp}}\right)^{1/3} - 1. \quad (35)$$

The obtained relative supersaturation value $\sigma = 157$ is consistent with the data presented in the literature [2, 25]. A high supersaturation value for systems in which sparingly soluble substances are crystallized by means of a chemical reaction is confirmed.

5.2. Nucleation Sources. If during the precipitation process such a huge value of the relative supersaturation ($\sigma = 157$) is generated, one may expect, despite the crystals' attrition, that the primary nucleation may be a dominant source of nuclei. Question is only, what type of this nucleation, e.g., heterogeneous or homogeneous is in majority. In order to find the answer to the presented question, the Mersmann's and Kind's work [2, 25] was taken into consideration. The mentioned authors, in the light of a huge number of experiments and observations, have determined a critical value of supersaturation (for different solubilities c^*) up above which the homogeneous primary nucleation takes place. According to this, they have created a chart $\Delta c_{\text{crit}_{\text{hom}}} = f(c^*)$ divided into homogeneous and heterogeneous zones (valid for an average molecule diameter $d_{\text{mol}} = 4.6 \cdot 10^{-10}$m, average diffusivity $D_{AB} = 2 \cdot 10^{-9}\,(\text{m}^2/\text{s})$, and interfacial tensions γ_{Sl} that may be estimated according to Nielsen's and Söhnel's work [26]). They have also marked the range of the most frequently used supersaturations for which crystallization studies were carried out (the hatched area). On the basis of the discussed chart, with the knowledge of such parameters as solubility c^* and the relative supersaturation σ, it is possible to determine in which zone the analyzed process is located.

In accordance with the presented information, the obtained experimental data ($\sigma = 157$ and the c^* calculated on the basis of the solubility product $K_{sp} = 3.55 \cdot 10^{-11}\,(\text{kmol/m}^3)^3$ from equation (13) what gave $c^* = 2.07 \cdot 10^{-4}\,(\text{kmol/m}^3)$) were transferred to the discussed graph (Figure 5).

As presented in Figure 5, the location of the marked working point suggests that the supersaturation of the solution generates, in the considered case, the heterogeneous primary nucleation and the marked point layers in the mostly occurring range of precipitation processes, as well.

5.3. The Mechanism Controlling the Crystal Growth. In order to determine the controlling step in the considered case of CaF_2 precipitation, the required calculations, described in details in the theory section, were made. The data used for this purpose are collected in Table 4.

On the basis of the presented data (Table 4), the conditions showed in equations (10) and (11) were checked. The results are as follows:

(1) $0.01 \cdot \sqrt{c_c/c^*} = 4.38 \longrightarrow \sigma = 157 > 4.38 \longrightarrow$ the condition is met

(2) $2 \cdot 10^{-4} \cdot \sqrt{c_c/c^*} = 0.08 \longrightarrow \sigma = 157 > 0.08 \longrightarrow$ the condition is not met

For the conditions presented in the paper ($\sigma = 157$), only the first requirement is fulfilled. It means that the

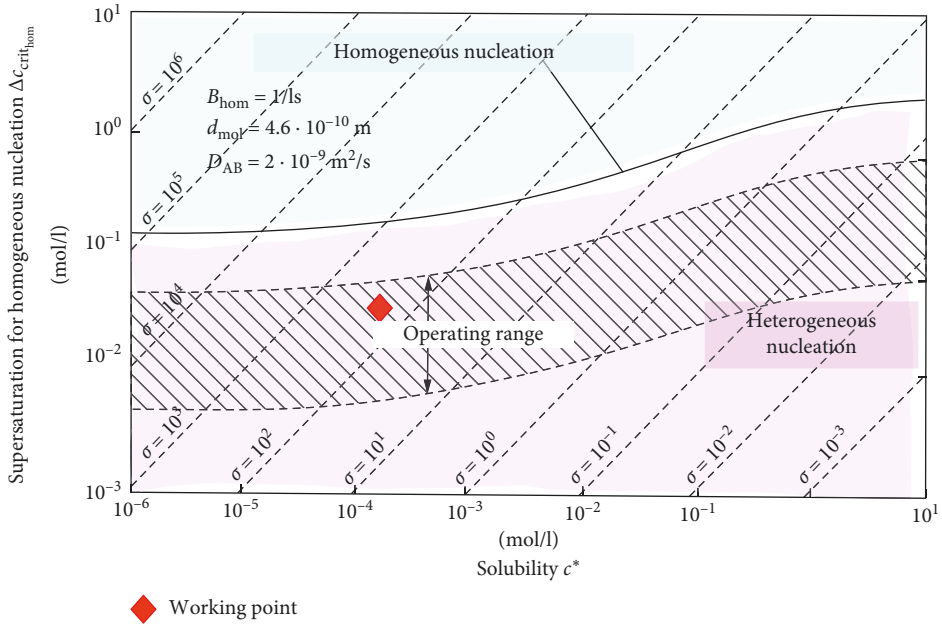

Figure 5: Ranges of homogeneous and heterogeneous nucleation [2] with the marked working point from CaF_2 precipitation.

Table 4: Calculation data.

Property	Value
Molar mass (kg/kmol)	$M_{CaF_2} = 78$
Density (kg/m^3)	$\rho_{CaF_2} = 3180$
Solubility product at 25°C ((kmol/m^3)^3)	$K_{sp} = 3.55 \cdot 10^{-11}$
Relative supersaturation (–)	$\sigma = 157$
Solubility (kmol/m^3)	$c^* = 2.07 \cdot 10^{-4}$
Molar density of crystals (kmol/m^3)	$c_c = 40.77$

precipitation of CaF_2 carried out in the experimental work is limited by the bulk diffusion. Such an observation is consistent with the plot presented by Mersmann et al., [21] which clearly states that for $\sigma = 157$ and for the ratio $c^*/c_c = 5 \cdot 10^{-6}$, the crystal growth controlling step is bulk diffusion. For visualization of the obtained results, Figure 6 is presented.

5.4. Influence of Fluid Dynamic Conditions on the Conversion Rate of Fluorides Removal. The calculation of the conversion rate was based on the initial and final concentrations of fluorides in the feed solution of NH_4F and in the obtained mother liquor, in accordance with the following equation:

$$\eta = \frac{C_{F^-_{init}} - C_{F^-_{fin}}}{C_{F^-_{init}}} \cdot 100\,(\%). \quad (36)$$

The obtained results are presented in Figure 7.

As presented, in all of the investigated cases, the conversion rate of fluoride ions removal is really high ($\eta > 97\%$) even at the lowest Reynolds number. What is more, the difference between η in the laminar and turbulent flow regimes is really small (in Kenics 0.87%, in Koflo 0.16%, and in a pipe 0.89%, respectively). It means that, in the investigated range, the considered reaction fluid dynamic

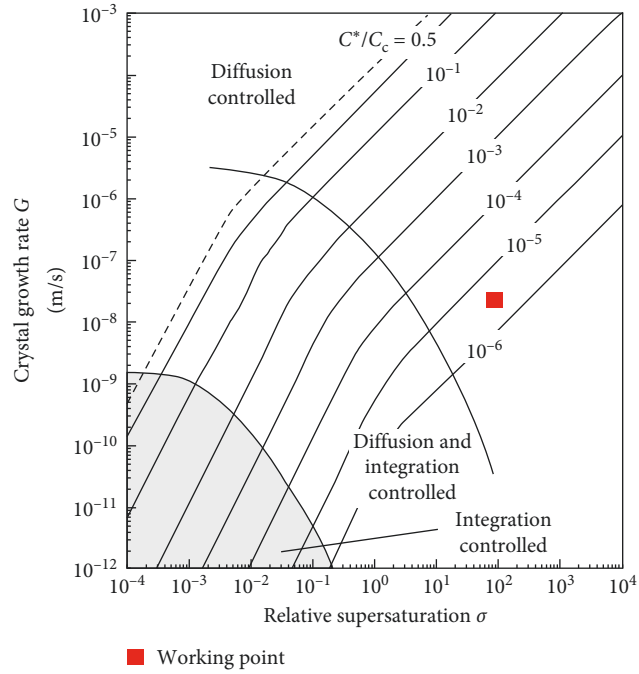

Figure 6: Control mechanisms of crystal growth rate [21] with an additional working point referring to the analyzed process and conditions.

conditions (represented by the Reynolds number) do not play a significant effect on the conversion rate. Therefore, from an economic point of view, it would be suggested to run the process at low velocities to reduce energy consumption significantly [15].

On the contrary, if the comparison between the static mixers and a pipe would be made, it could be observed that the use of static mixers allows obtaining a higher conversion

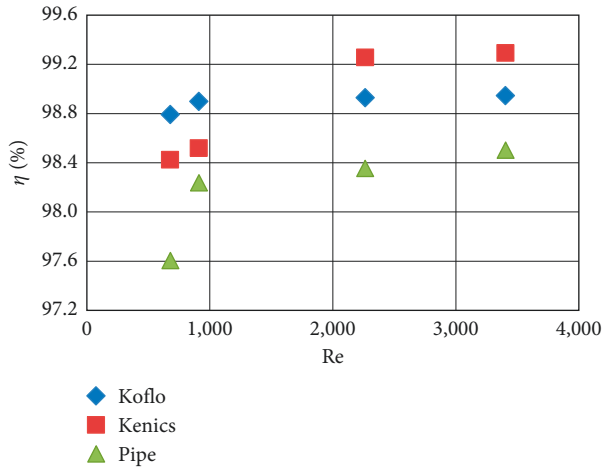

Figure 7: The conversion rate of fluorides removal as a function of the Reynolds number.

rate than the one achieved by the use of a pipe. It is particularly noticeable in the laminar flow (the lowest Reynolds number), and it may be explained on the basis of mixing degree. As mentioned in the paper [13], the CoV in the pipe in the laminar flow regime was at a higher level (CoV ~ 13%) than allowable (CoV > 5%) and this fact is reflected in the reduction of conversion rate. For transient/turbulent flows (Re > 2300), the situation is different. There the CoV was about 1% which means that the mixture at the pipe's outlet could be considered as homogeneous. In turn, it translates into an increased conversion rate.

In the case of static mixers, the experiments showed that their use allows obtaining the highest degree of mixing. Values of the CoV were less than 1% in both laminar/transient and turbulent flows which prove the versatility of their application. The existence of mixing elements clearly helps in the mixing operation causing "artificially made" swirls and vortexes which effect in an increase of mixing degree. On the contrary, when the rheology of fluid is close to water, the structures that naturally occur in the turbulent flow cause the reduction of the CoV all by themselves and make a simple pipe a useful alternative to more expensive static mixers, especially in case of not very demanding processes [13].

5.5. CSD (Crystal Size Distribution): The Secondary Nucleation or Variable Conditions of the Primary Nucleation? In accordance with the performed laser particle size analyses for the obtained samples of CaF_2 crystals, the solid product was evaluated on the basis of the determined particle density distribution q_3 and particle undersize distribution Q_3. Some of the obtained curves are presented in Figures 8–10.

In turn, the population density of crystals $n(L)$, defined as the number of crystals per size and per volume unit of bed, that may be calculated on the basis of (equation (37)) in each size class, was presented in Figures 11–13 for the pipe, Koflo, and Kenics, respectively:

$$n(L_i) = \frac{w_i \cdot \phi}{k_v \cdot L_i^3 \cdot \Delta L_i} \left(1/\mathrm{m}^4\right). \tag{37}$$

In accordance with the presented data (Figures 11–13), it may be observed that the range of crystal sizes changes considerably with the change of fluid dynamic conditions. Therefore, a question is arising: what is the reason for these changes? More specifically, are they caused by the variable conditions of primary nucleation or maybe their cause is connected with crystals' destruction resulting from secondary nucleation?

In all of the measurements carried out, the relative supersaturation σ was constant (and its value was equal to 157). It was dictated by the assumed reagents' concentrations and the solubility product K_{sp}. Such conditions generated the primary nucleation with the same intensity in all of the provided experiments. The local changes of supersaturation, and consequently, changes in primary nucleation conditions, could be affected by the so-called micromixing effect (mixing at the molecular level). Because of the fact that, in the considered static mixers, the distribution of energy dissipation rate ε, even for low Reynolds numbers, is very uniform (it means that the local values are close to the averaged one $\varepsilon_{lok} \approx \varepsilon_{śr}$)—what is evidenced by CFD simulations (Figures 14 and 15), it is shown that the impact of the micromixing on the primary nucleation is more than less constant in a whole volume of a mixer.

To confirm a predicted influence of micromixing on the primary nucleation, a comparative analysis between the induction and micromixing times (calculated from the following equations) was made, and the results are presented in Table 5:

$$\tau_{\mathrm{ind}} \approx \frac{80 \cdot d_{\mathrm{mol}}^2}{D_{\mathrm{AB}} \cdot \ln(S)}\,(\mathrm{s}), \tag{38}$$

$$\tau_{\mathrm{mic}} = 50\sqrt{\frac{\nu}{\varepsilon_{\mathrm{loc}}}} \cdot \ln(\mathrm{Sc})\,(\mathrm{s}), \tag{39}$$

where $d_{\mathrm{mol}} = 4.6 \cdot 10^{-10}\mathrm{m}$ is an average molecule diameter and $D_{\mathrm{AB}} = 2 \cdot 10^{-9}\,(\mathrm{m}^2/\mathrm{s})$ is an average diffusivity [2].

If the induction time would be greater than the micromixing time $\tau_{\mathrm{ind}} > \tau_{\mathrm{mic}}$, then the variable fluid dynamic conditions of flow caused by micromixing accelerates effectively the primary nucleation rate. Otherwise, for $\tau_{\mathrm{ind}} < \tau_{\mathrm{mic}}$, the effect of micromixing on the primary nucleation rate is stable, and the observed huge changes in the nucleation rate may be caused by means of attrition phenomenon, which also determines the change in the size of the obtained crystals [27, 28].

As presented in Table 5, in all of the considered cases, the induction time was much lower than the micromixing time. It means that the micromixing effect has limited effect on the primary nucleation changes. That is why it can be stated that the strong influence between the CSD and fluid dynamic conditions (represented by the Reynolds number) is caused mainly by crystals destruction (or in other words by the secondary nucleation).

An additional confirmation of the secondary nucleation effect on the final crystal size is the analysis of nucleation intensity B_0. The calculations of nucleation rates were made on the basis of the following equation, and the obtained results are presented in Table 6.

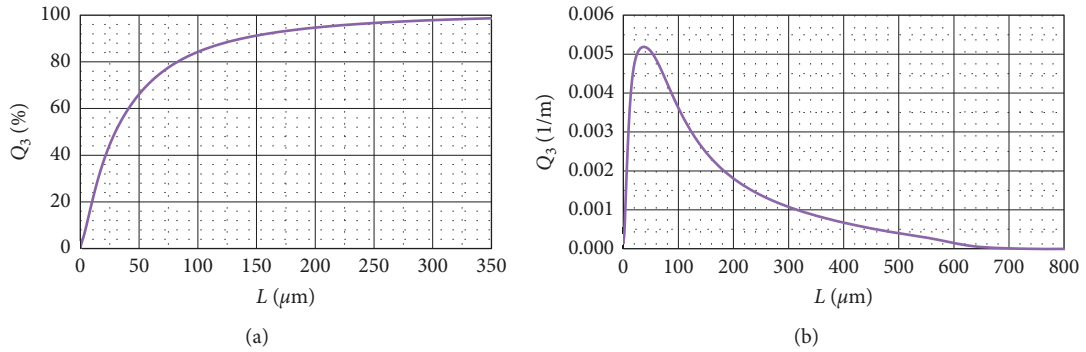

Figure 8: Particle distributions obtained by the use of a pipe for Re = 3404.

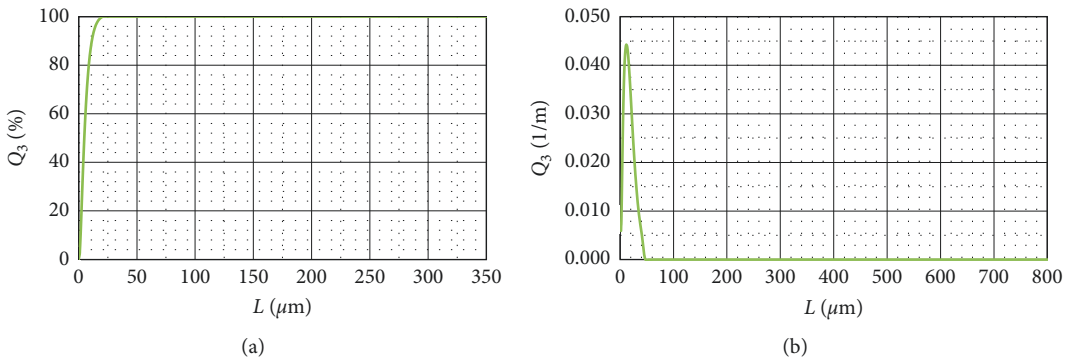

Figure 9: Particle distributions obtained by the use of Koflo static mixer for Re = 3404.

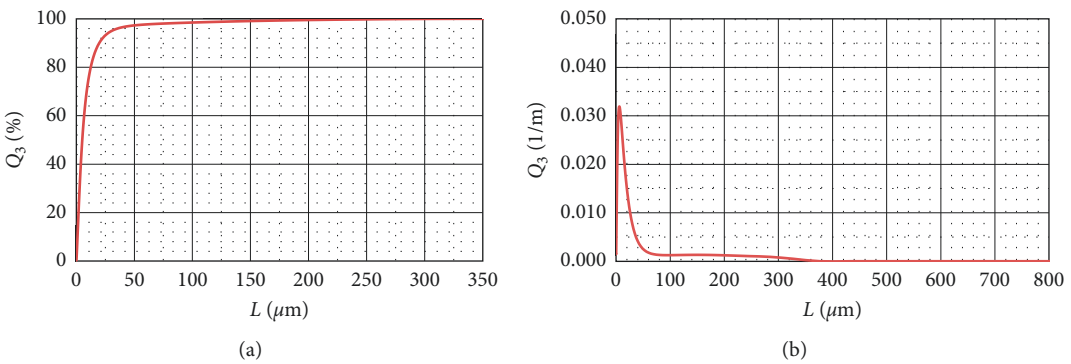

Figure 10: Particle distributions obtained by the use of Kenics static mixer for Re = 3404.

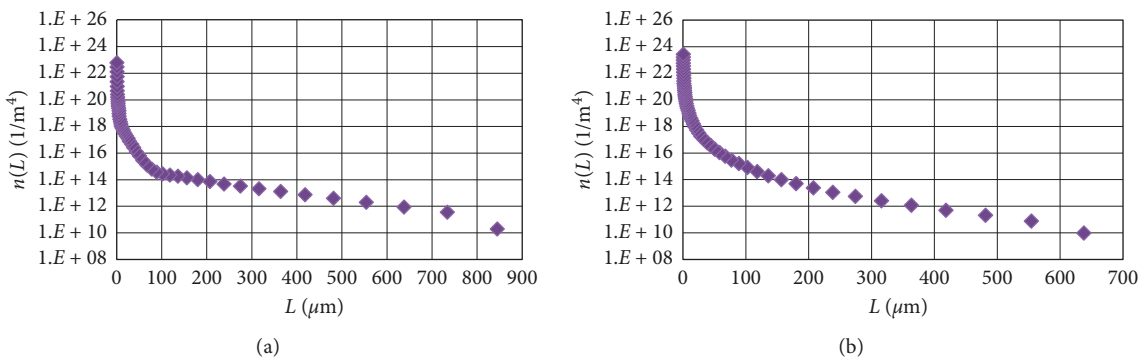

Figure 11: Population density $n(L)$ obtained by the use of a pipe: (a) Re = 677; (b) Re = 3404.

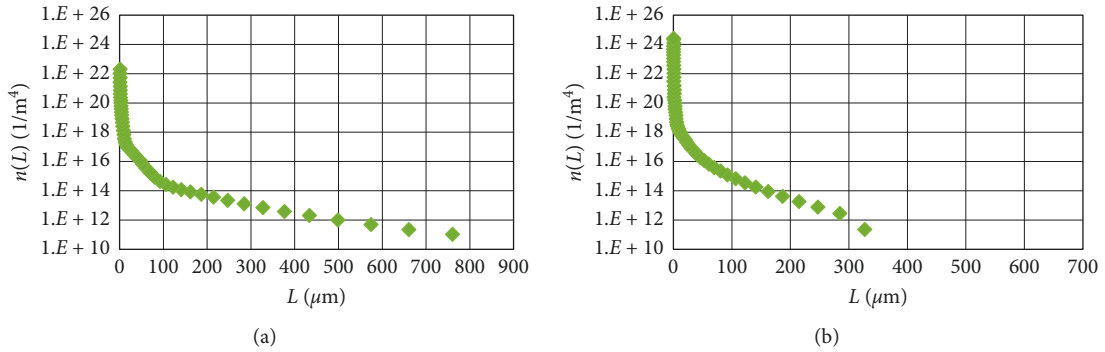

Figure 12: Population density $n(L)$ obtained by the use of Koflo: (a) Re = 677; (b) Re = 3404.

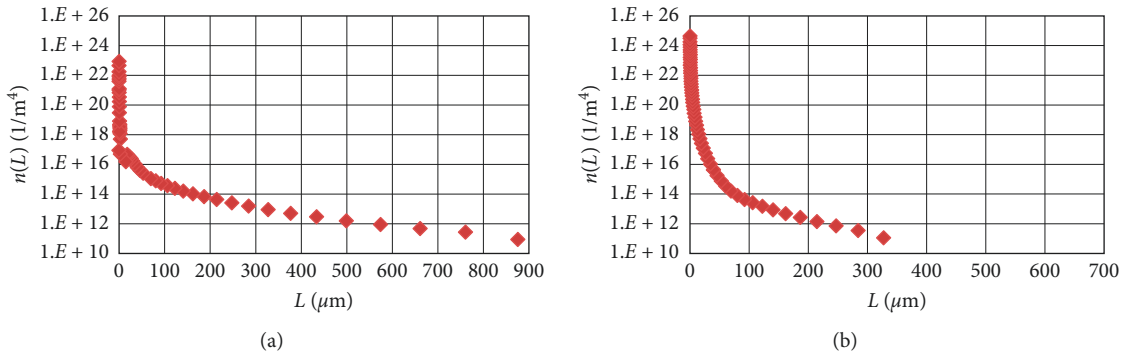

Figure 13: Population density $n(L)$ obtained by the use of Kenics: (a) Re = 677; (b) Re = 3404.

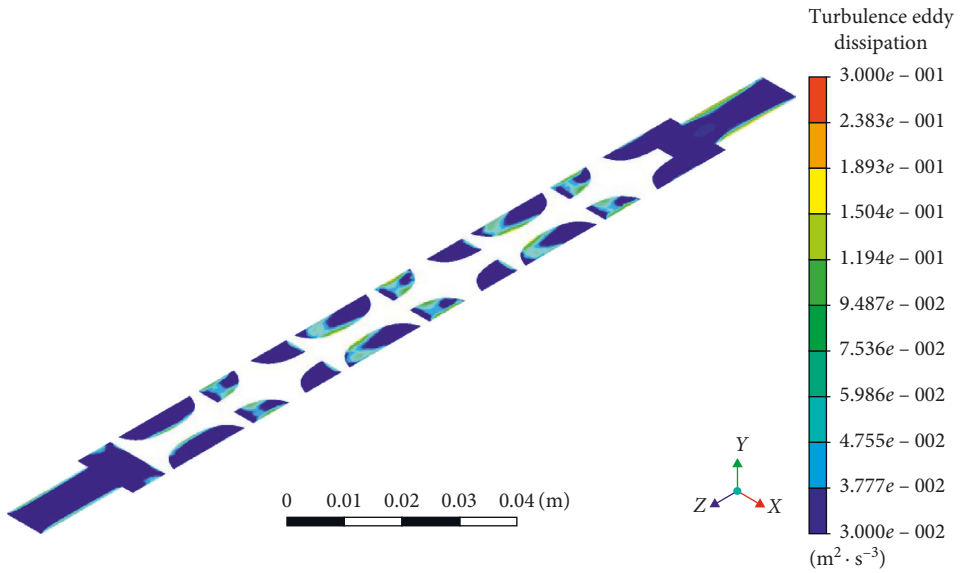

Figure 14: The energy dissipation rate ε in the Kenics static mixer (Re = 677).

$$B_0 = n_0 \cdot \left(\frac{L_{\text{mean}}}{t_{\text{m}}}\right)\left(1/\text{m}^3 \cdot \text{s}\right). \tag{40}$$

As shown in Table 6, the fluid dynamic conditions have a significant influence on the nucleation intensity. When the Reynolds number increases, the value of B_0 increases and it is caused mainly by the increasing mixing intensity. In the transient/turbulent flow, due to a higher fluid velocity and the presence of a large number of swirls and vortexes, the mixed streams collide with each other in a much more rapid manner than in the laminar flow, which in turn leads to the generation of a greater number of nuclei.

What is more, when comparing the intensity of nucleation in the considered devices (Table 6), it can be observed that, in the pipe, the lowest values of B_0 are obtained. If it is about the static mixers, they remain rather at a similar level

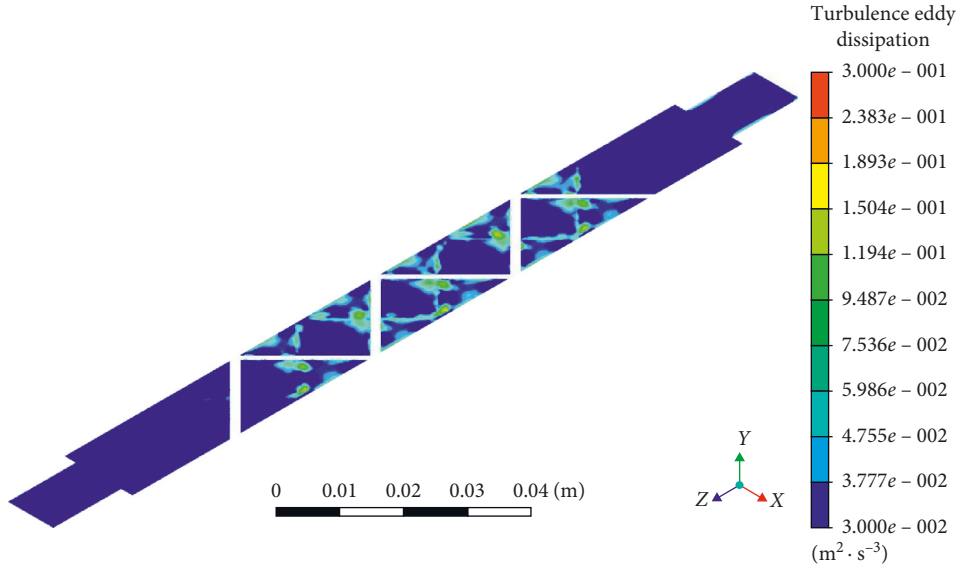

Figure 15: The energy dissipation rate ε in the Koflo static mixer (Re = 677).

Table 5: The comparison of the induction and micromixing times.

Re	σ $S = 1 + \sigma$	τ_{ind} (s) (Koflo and Kenics)	τ_{mic} (s)	
			Koflo	Kenics
677	157 ($S = 158$)	$1.73 \cdot 10^{-9}$	$1.48 \cdot 10^{0}$	$1.08 \cdot 10^{0}$
911			$9.21 \cdot 10^{-1}$	$6.63 \cdot 10^{-1}$
2261			$2.51 \cdot 10^{-1}$	$2.51 \cdot 10^{-1}$
3404			$1.42 \cdot 10^{-1}$	$1.44 \cdot 10^{-1}$

Table 6: The relation between Reynolds number and the nucleation rate B_0.

Re	B_0 ($m^{-3} \cdot s^{-1}$)		
	Koflo	Kenics	Pipe
677	$\mathbf{9.1 \cdot 10^{18}}$ (δ_{av} 6.9%)	$\mathbf{1.1 \cdot 10^{19}}$ (δ_{av} 9.2%)	$\mathbf{6.0 \cdot 10^{18}}$ (δ_{av} 5.1%)
3404	$\mathbf{7.9 \cdot 10^{19}}$ (δ_{av} 26.1%)	$\mathbf{8.4 \cdot 10^{19}}$ (δ_{av} 27.3%)	$\mathbf{1.4 \cdot 10^{19}}$ (δ_{av} 24.8%)

(with a slight advantage of a Kenics static mixer). In accordance with the presented data, it becomes clear why the destruction of crystals in the pipe is at a lower level. Namely, the change in the nucleation intensity (with a constant value of $B_{0_{prim}}$) is influenced by the value of $B_{0_{second}}$. Due to the lack of mixing elements in the pipe (there are no crystal-static inserts collisions), the probability of mechanical collisions between crystals is much lower than in the case of static mixers (according to a larger effective volume) and thus, the intensity of a nuclei generation due to secondary nucleation is also lower. In turn, less intense destruction means larger final crystal size. Such a conclusion is consistent with the experimental data presented in Figure 16, where the mean crystal size (designated on the basis of the data obtained from the laser analyzer) was shown as a function of fluid dynamic conditions represented by the Reynolds number.

In case of static mixers, the intensity of secondary nucleation $B_{0_{second}}$ is at a similar level, and hence, the obtained crystals sizes, particularly in the turbulent flow, are close to each other (Figure 16).

As shown in Figure 16, in all of the investigated cases, the mixing intensity strongly influences the CSD. The mean crystal size decreases with an increasing Re number value. In the analyzed static mixers, the mentioned effect of Re on CSD was almost similar. What is interesting, the precipitation carried out in stirred tanks did not show so strong relation between CSD and fluid dynamic conditions. In the present investigations, the influence of the unit power input on the final particle size is described by the following relation $L \propto \varepsilon^{-0.38}$: when in mechanically stirred reactors, it may be written that $L \propto \varepsilon^{-0.23}$ [29–31]. The explanation of that fact is connected mainly with the supplied power input value. In the mechanically agitated crystallizers, the unit power input very rarely exceeds the value of 1 W/kg in the turbulent range of flow, while in static mixers in this same flow regime, the unit power input reaches 10 W/kg. Knowing that ε is proportional to the energy of destruction, one may find an explanation of more intensive crystal attrition in static mixers.

It is worth mentioning that it was also observed that agglomeration phenomenon was in minority (Figures 11–13). The crystal shape and the mean size strongly depend on flow conditions, and it may be written as follows:

(i) For Kenics $L_{mean} \propto \mathrm{Re}^{-1.97}$

(ii) For Koflo $L_{mean} \propto \mathrm{Re}^{-2.05}$

(iii) For the pipe $L_{mean} \propto \mathrm{Re}^{-0.85}$ only

What is more, the SEM microscopy observations (Figures 17–19) show that not only the CSD strongly depends on fluid dynamic conditions but also the shape of crystals is a dependent variable. Such an observation led to the conclusion that the obtained solid particles differ from each other with the volumetric shape coefficient k_v. To

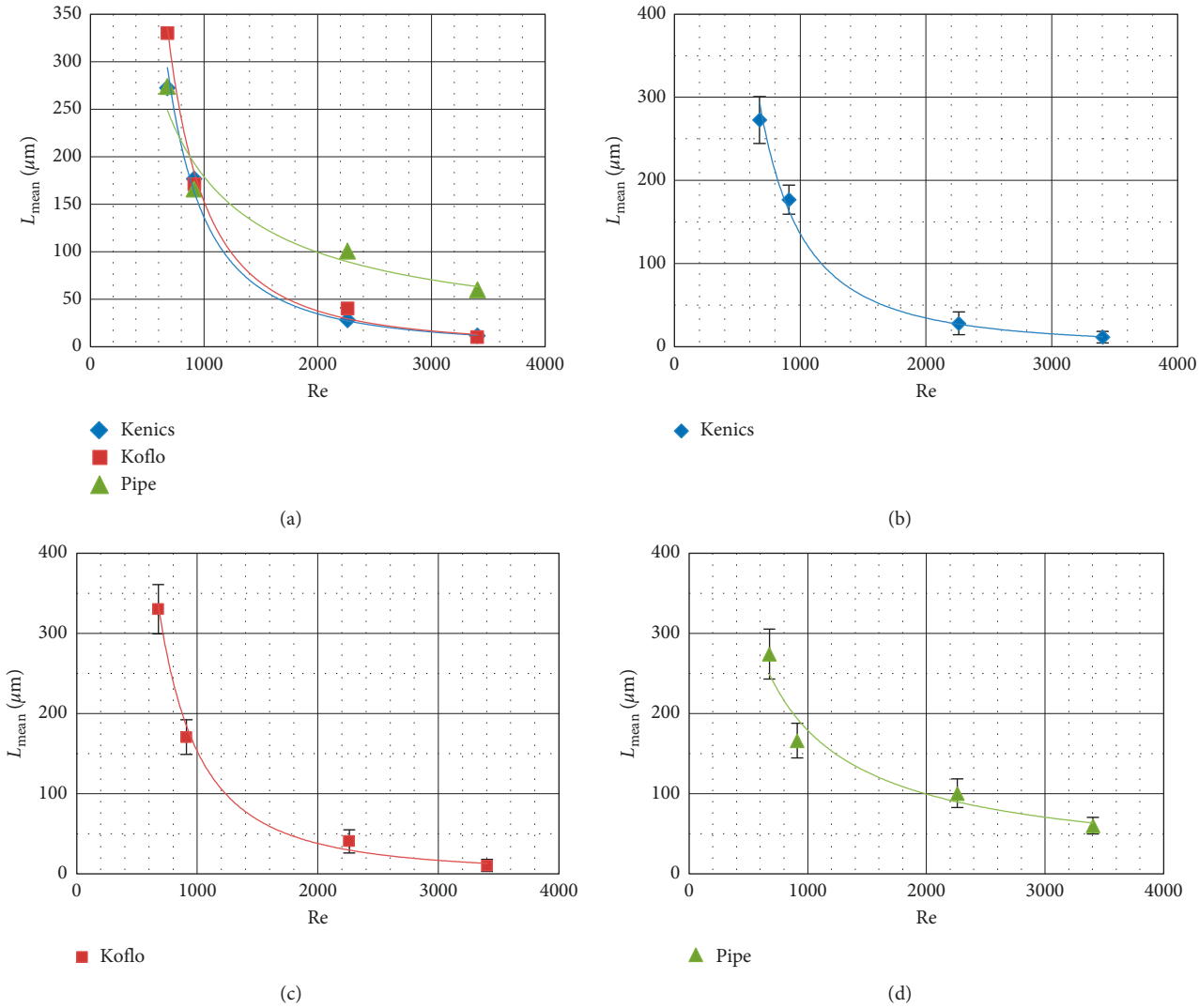

Figure 16: (a) The effect of the Reynolds number on the mean crystal size: plots with scatter bars showing the standard deviations from the mean crystal size of (b) Kenics, (c) Koflo, and (d) pipe.

obtain its value in the considered conditions, SEM observations and measurements were used. The results of the k_v are presented in Table 7.

On the basis of the values collected in Table 7 and presented SEM photo samples (Figures 17, 18, and 19), it may be concluded that the conditions of growth changes when Re number is increased. For a low value of the Reynolds number, crystals become flat and thin and k_v reaches 0.35. When Re approaches 3000 and more, the shape of precipitate becomes more orthogonal with the k_v coefficient bigger than 0.94.

5.6. The Relation between Fluid Dynamic Conditions and the Particle-Size Distribution. As suggested, the provided experiments considered in the presented paper proved the existence of intensive attrition phenomenon in CaF_2 crystals.

The highest effect of Re number on attrition was observed in the Koflo static mixer. The size of particles was reduced from 330.1 to 10.3 μm, while in Kenics from 272.7 to 11.6 μm, and in an empty pipe, from 274.2 to 59.8 μm (Figure 16).

In this specific situation, it is very difficult to distinguish what is the main cause of crystal size reduction when the Reynolds number is increased because the increase of the Reynolds number results in the increase of destruction rate and reduction of the residence time. And those two factors negatively influence the final product size. In practice, it is impossible to separate those parameters, as, for example, keeping the residence time constant when Re is increased requires the use of a longer mixer, which, in turn, results in the increased number of crystal-inserts collisions.

5.6.1. Crystals' Destruction Sources. It should be highlighted that the proposed model for the destruction description is valid in any kind of flow, i.e., laminar, transient, and turbulent, respectively.

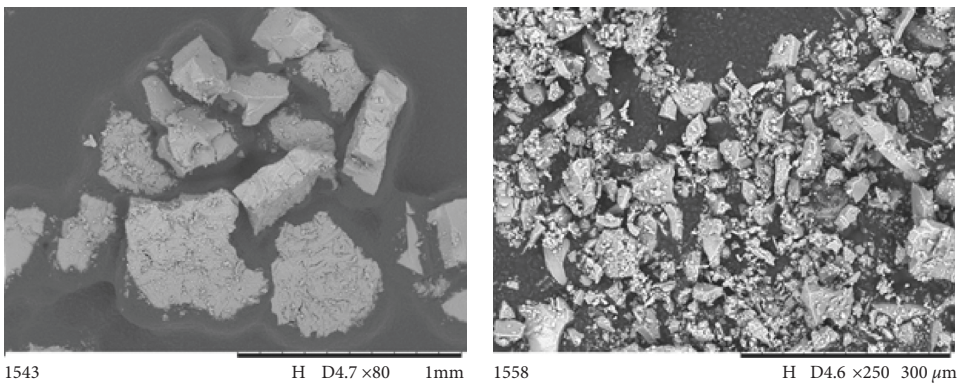

Figure 17: CaF_2 particles after precipitation in the Kenics static mixer: (a) Re = 677; (b) Re = 3404.

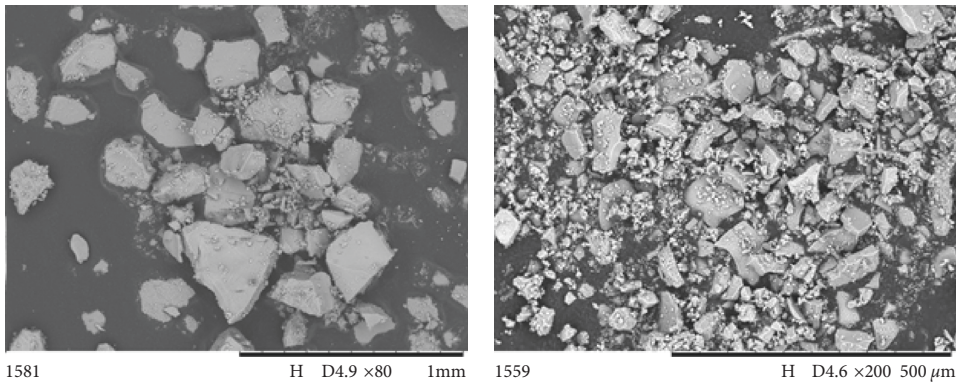

Figure 18: CaF_2 particles after precipitation in the Koflo static mixer: (a) Re = 677; (b) Re = 3404.

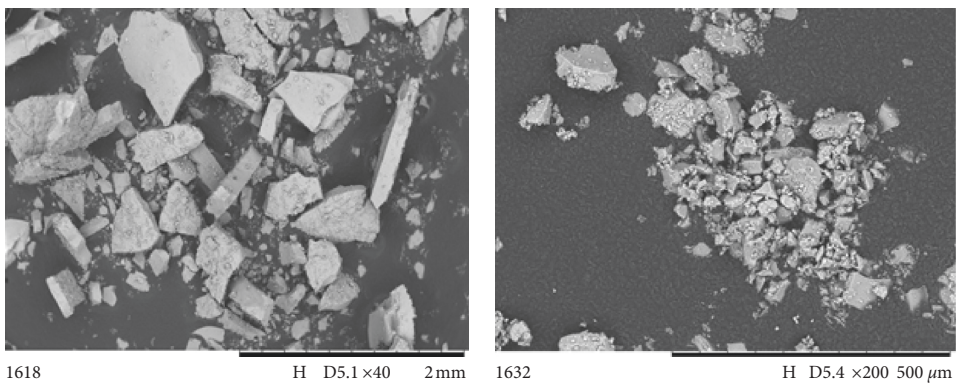

Figure 19: CaF_2 particles after precipitation in the pipe: (a) Re = 677; (b) Re = 3404.

Table 7: The volumetric shape coefficients for the obtained crystals.

Re	k_v		
	Koflo	Kenics	Pipe
677	0.347	0.532	0.458
911	0.542	0.603	0.697
2261	0.736	0.786	0.755
3404	0.943	0.968	0.972

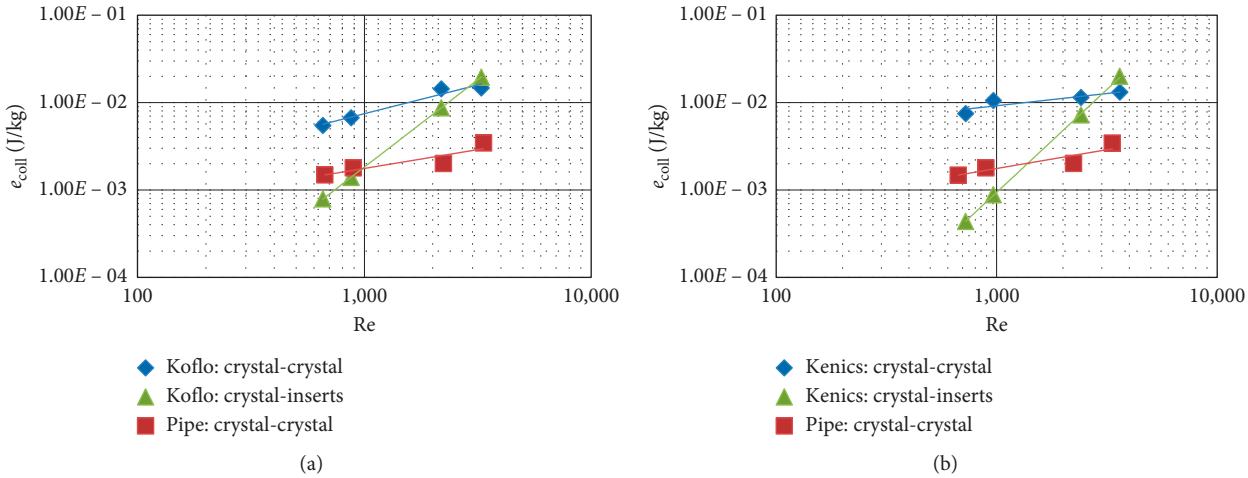

Figure 20: Mechanical collisions in static mixers and pipe for $L_m/d = 12.4$: (a) the comparison of Koflo and a pipe; (b) the comparison of Kenics and a pipe.

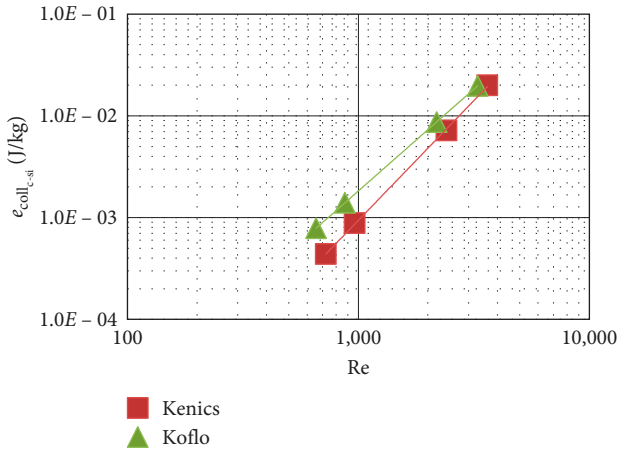

Figure 21: The unit energy caused by mechanical collisions between crystals and static inserts.

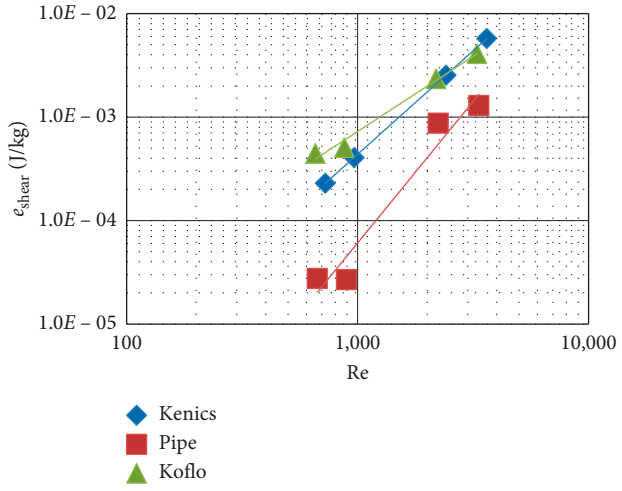

Figure 22: The comparison of the unit shear energy in the tested devices.

During the experiments, static mixers stayed in the laminar (Re < 1000) and turbulent range of flow (Re > 1000) [32, 33], while the pipe was working in the laminar and transient regimes (Re < 4000) [32]. In static mixers, the mechanical collisions may be generated by both crystal-crystal collisions and crystal-static inserts. However, in the empty pipe, mostly the crystal-crystal collisions exist.

In accordance with formulas mentioned in the theory section (equations (14)–(21)), the particular unit destruction energies were calculated. As an illustration of the obtained results, Figures 20–22 are presented as follows.

As presented in Figure 20, in both static mixers, for the Reynolds numbers less than 3000, the crystal-crystal collisions play a dominant role in the mechanical destruction. For higher values of the Reynolds number, the crystal-inserts collisions mainly influence the CSD. On the contrary, if the pipe would be considered, then it may be observed that the unit energy of crystal-crystal collisions ($e_{c\text{-}c}$) is about 40% lower than the ones obtained in mixers. The main cause of such a difference lies in the different flow behaviors in the devices like static mixers and a pipe. In the examined Reynolds number range, the pipe works in the traditional laminar/transient flow. In static mixers, the laminar flow is only hypothetical because the parallel layers in which the fluid flows do not exist because of the static inserts presence (more detailed explanation about the different flow regime definitions for considered devices may be found in [12]). Therefore, the flow in static mixers has more artificial swirls and vortexes, so it has more energy to dissipate. That is why the collisions between crystals in static mixers are more energetic than the ones obtained when the pipe is used.

What is more, if the comparison between the crystal-static inserts collisions in both static mixers would be made (Figure 21), then it could be observed that Koflo is characterized by a higher value of unit energy destruction. The explanation is connected with the geometry of mixers. Helices present in Kenics have much streamlining shape, and the approach angle is smaller ($\alpha_{Kenics} = 30^\circ$, $\alpha_{Koflo} = 45^\circ$), so the crystals hit

the inserts with less force. In Koflo, inserts are more angular and impede the flow resulting in more destructive collisions.

The calculation of the unit shear energy was based on equations (19)–(21). As the local energy dissipation rate, the average value was assumed. Such an assumption was possible to make because on the basis of the authors' CFD calculations, it was proved that the distribution of ε in the mixers is very uniform (even for low Re numbers) and is close to the average value, as presented in Figures 14 and 15.

What is important, from Figure 22, it may be seen that, in the considered conditions, the value of the unit shear energy is almost seven times higher in static mixes than the one obtained by use of a pipe. The explanation, just like in mechanical crystal-crystal collisions, is connected with the different flow regime definitions. Additionally, in the whole investigated range of the Reynolds numbers, the shear unit energy is ten times smaller than the mechanical unit energy of collisions. It shows that the shear stresses do not play an important role in crystals' destruction.

To sum up and clearly state what is the main source of the destruction, the sum of unit destruction energies ($e_{\text{c-c}}$ and e_{shear} in case of a pipe and $e_{\text{c-si}}$, $e_{\text{c-c}}$, and e_{shear} in case of static mixers) was calculated. The results are shown in Figures 23 and 24.

As presented in Figures 23 and 24, in the case of static mixers, the key role as a destruction source plays mechanical collisions (for $\text{Re} < 3000$, the major contribution belongs to crystal-crystal collisions, and for $\text{Re} > 3000$, crystal-inserts collisions (Figure 20)). The other destruction sources, like shear stresses, may be neglected in calculations due to a very low value in comparison to the mechanical destruction.

If the pipe would be considered, it could be written that the main source of a destruction has crystal-crystal mechanical collisions. What is more, just like in static mixers case, there is "no sign," so their contribution may be also neglected.

5.6.2. The Effective Energy of Crystals' Destruction. The analysis of the possible ways in which crystals may be destroyed was presented separately for the residence time and destruction sources causes. However, these two factors affect the destruction of crystals simultaneously. That is why, as mentioned in the theory section, the authors propose to calculate the effective destruction energy (equation (22)), which takes into account both destruction causes.

In accordance with the presented procedure, the frequency of interactions and the effective destruction energy have been calculated and the obtained results are shown in Figures 25 and 26, respectively. To facilitate the interpretation of the presented data, the table with the collection of mean residence times is attached (Table 8).

As demonstrated in Figure 25, the frequencies of both mechanical collision types (c-c and c-si) in Koflo and Kenics static mixers stay almost at the same level (with a slight advantage of the Koflo static mixer where the frequencies are a little bit lower). The explanation of such a behavior is closely related to the used frequency definitions (equations (23) and (24)). Let us first consider the crystal-static inserts collisions (equation (23); Figure 25(b)). For the same volumetric flow rate and smaller elemental volume V_{i} in the Kenics static mixer (in comparison to Koflo), the obtained frequency value is slightly higher. If the crystal-crystal collisions would be considered (equation (24); Figure 25(a)), the main factor which affects the frequency value is the inverse mean crystal size in the power of 2/3 ($1/L_{\text{mean}}^{2/3}$). In the Kenics static mixer, the obtained crystal sizes were smaller than the ones from Koflo (Figure 16). It means that their inertia is greater and that results in the greater probability of collisions. Moreover, in the analyzed range of the Reynolds numbers, static mixers stayed in the turbulent regime, where swirls and vortexes are present. Thanks to that, there is a recombination of fluid paths in radial and tangential directions which lead to the increasing number of interactions between crystals. In turn, if the pipe would be taken into account, it is clear that the frequency of crystal-crystal collisions is lower than the ones in static mixers. In the pipe, there are no flow interrupters and the volume of fluid is greater. If the volume is greater than the probability of crystals, collisions are lower because the particles do not have to "fight" for the space to reach the outlet.

What is more, it can be observed that the frequencies of crystal-crystal collisions are about 5–80 times higher than crystal-static inserts collisions. It means that the selected static mixers' geometries have so streamlining shape that crystals flow freely in the fluid stream (it may be assumed that the solid particles are small enough that their velocity is approximately equal to the velocity of fluid) between consecutive static inserts. That is why the collisions between crystals and mixing elements are rather random and take place when the solid particle flows out from the path line.

According to the provided frequencies analyses, it may be expected that the effective energy of crystal-crystal collisions would be higher than the effective energy of crystal-static inserts collisions. Such a prediction is confirmed by Figure 26.

In turn, the value of total effective energy destruction will be similar to the effective energy of crystal-crystal collisions (Figure 27).

If now, the analysis of the effective mechanical energy destruction caused by crystal-static inserts collisions (Figure 26(b)) would be made, it is clear that Koflo shows higher values than Kenics. Despite the fact that $f_{\text{c-in}}$ is lower in Koflo, the mean residence time (the time of interactions) is higher and, what is more, as previously stated (Figure 21), the unit energy of crystal-static inserts collisions is also higher. That results in the higher $e_{\text{eff}_{\text{c-si}}}$. The situation is similar when the effective energy of crystal-crystal collisions is taken into account. The frequencies of crystal-crystal collisions are at comparable levels for Koflo and Kenics; however, Kenics shows higher $e_{\text{eff}_{\text{c-c}}}$. Even for the lower mean residence times t_{m}, the unit energies of crystal-crystal collisions are higher (Figure 20) and that affects the main result.

5.6.3. The Prediction of the Mean Crystal Size. For the prediction of the mean crystal size, the experiments were carried out for two additional lengths ($2L_{\text{m}}$ and $3L_{\text{m}}$) for Koflo and a pipe, respectively. For the gathered data, all the calculations aimed at the determination of the total

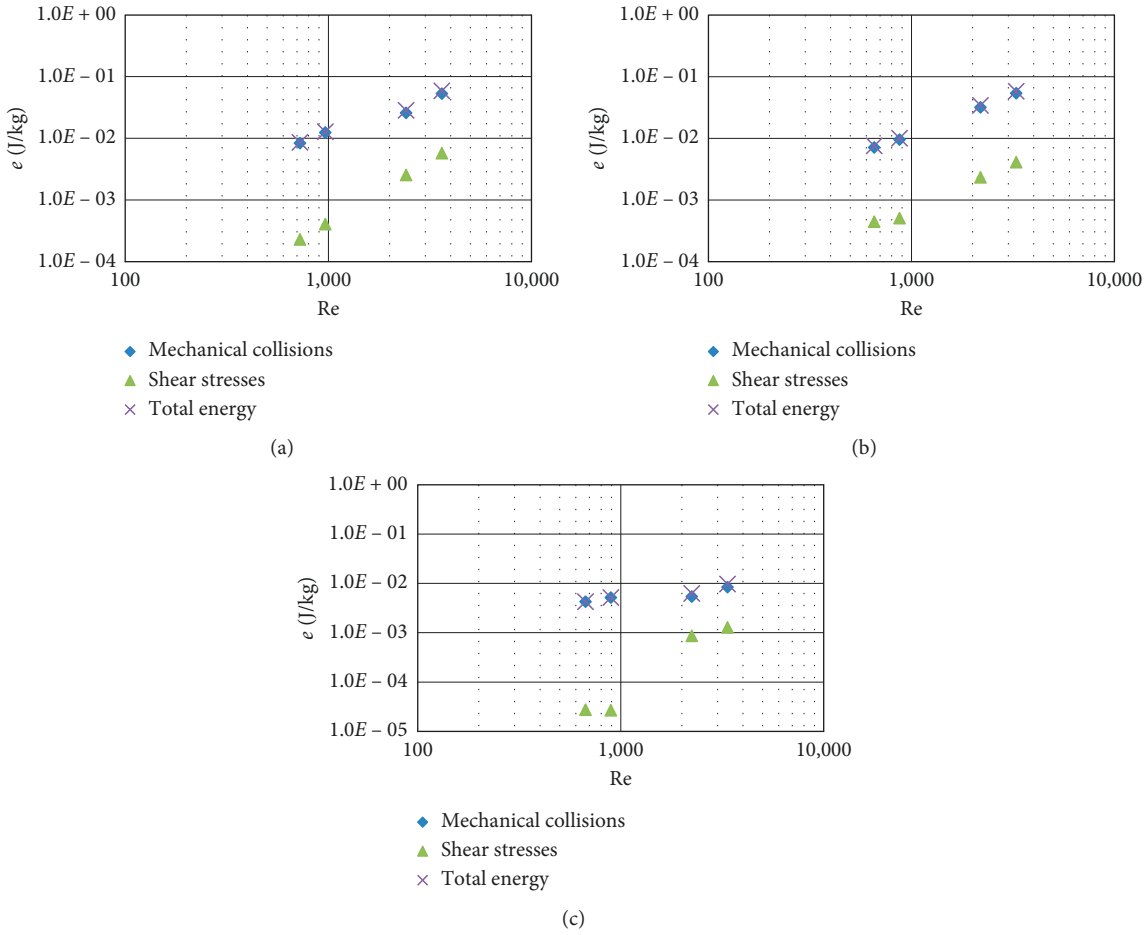

Figure 23: The contribution of individual destruction sources in the total unit energy: (a) Kenics static mixer; (b) Koflo static mixers; (c) pipe.

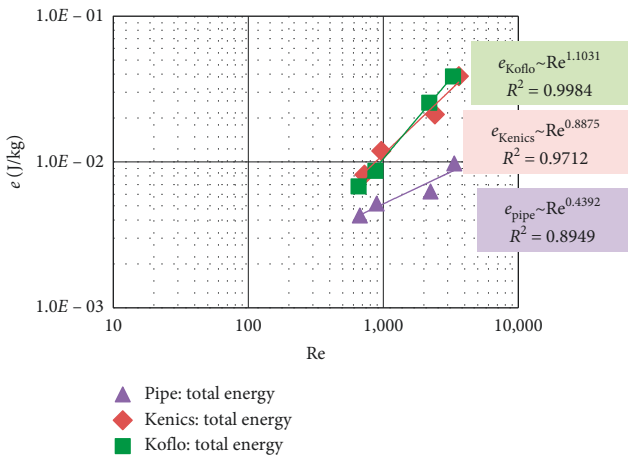

Figure 24: The comparison of total unit energy in the tested devices.

destruction energy (equations (28) and (29)) were made. The collection of the total destruction energies, as previously for two marginal Reynolds numbers, is shown in Table 9.

On the basis of the presented data (Table 9), it is clear why the mean crystal size changes with the change of L_m/d ratio. In all of the investigated cases, the total destruction energy increases with the increase of a device length. It is completely understandable because with the extended length, the mean residence time is extended, and the particles' traveling distance, at which the crystal-crystal collisions may occur, increases. What is more, the extended length in case of static mixers means the number of mixing elements increased, and therefore, the frequency of crystal-static insert collisions also increases.

For Re = 677, the total destruction energies are lower, and thanks to that the obtained particles are bigger. In the case of Re = 3404, the total destruction energy is higher. That is why the obtained crystalline products are much smaller than the ones obtained for the lower Reynolds numbers. What is more, the differences in total energies for different L_m/d ratios are lower, and the range of the crystal sizes are much narrower than for Re = 677.

If the derived model equation (28) or (29) correctly describes the mentioned phenomenon, one should find a relation between the particle size and the total unit energy destruction regardless of a mixer type.

For the verification of the above statement, a special plot was made (Figure 28). It shows a satisfying arrangement between the independently determined CSD and the presented theoretical model.

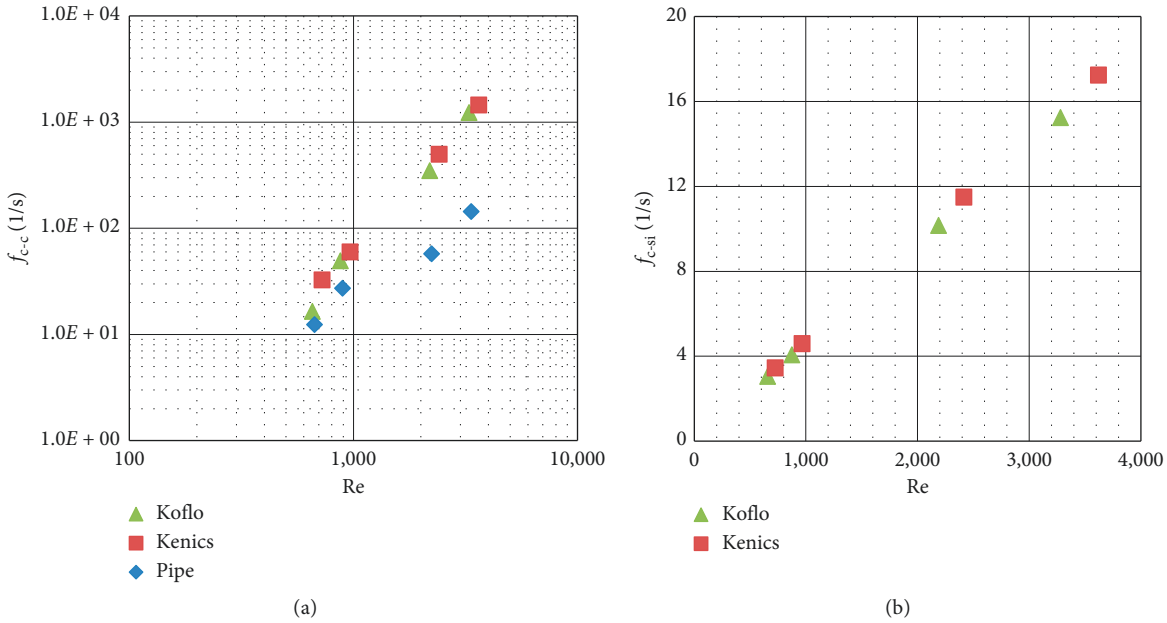

Figure 25: The frequency of interactions: (a) crystal-crystal collisions; (b) crystal-static inserts collisions.

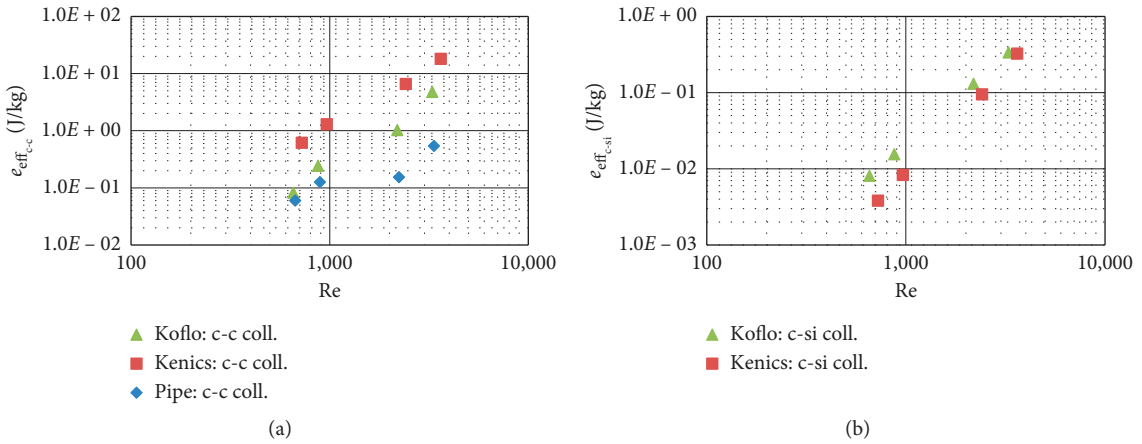

Figure 26: The effective mechanical energy destruction: (a) crystal-crystal collisions; (b) crystal-static inserts collisions.

Table 8: The collection of t_m values.

Re	t_m (s)		
	Koflo	Kenics	Pipe
677	3.36	2.52	3.26
911	2.73	2.05	2.58
2261	1.47	1.15	1.34
3404	1.12	0.95	1.09

We should be aware that the discussed model shows the destruction trends only and it has not been statistically elaborated.

Figure 28 shows that the effect of the total destruction energy e_{total} on a particle size is in the power of −0.47, which explains such big differences in the obtained mean crystals sizes.

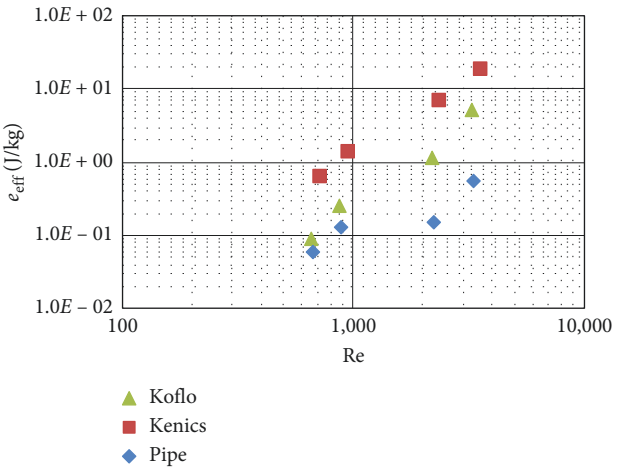

Figure 27: The total effective energy destruction.

Table 9: The collection of the total destruction energies.

L_m/d	Re = 677		Re = 3404	
	Pipe	Koflo	Pipe	Koflo
12.4	$5.99 \cdot 10^{-2}$	$9.05 \cdot 10^{-2}$	$5.42 \cdot 10^{-1}$	$5.10 \cdot 10^{0}$
18.67	$1.05 \cdot 10^{-1}$	$9.75 \cdot 10^{-2}$	$8.20 \cdot 10^{-1}$	$3.85 \cdot 10^{1}$
31.07	$1.70 \cdot 10^{-1}$	$2.13 \cdot 10^{0}$	$1.36 \cdot 10^{0}$	$6.43 \cdot 10^{1}$

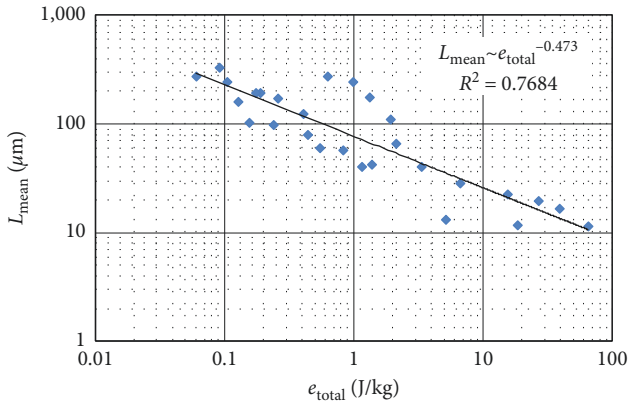

Figure 28: The mean crystal size as a function of the total destruction energy.

On the basis of the presented chart (Figure 28), it is possible to estimate the value of the mean crystal size independently from the mixer/pipe geometry. To do this, just the preliminary evaluation of the effective destruction energy is required. Admittedly, the relative error between the regression line and the proposed model is about ±34%, which may be treated as a satisfying result in this case.

In the author's opinion, spreading the investigations to other precipitated solids and taking into account some of the crystals' physical properties will enable in future to predict (anticipate) the mean particle size in relation to fluid dynamic conditions of flow.

6. Conclusions

The precipitation of sparingly soluble compounds in a static mixer is very specific. The unit power input is very uniform in comparison to the mechanically stirred reactors. The conversion rate is extremely high for all of the investigated range of the Reynolds values, but the mean particle size strongly depends on fluid dynamic conditions. This relation is much more visible than the one observed in a stirred tank. It shows, that by a precise determination of the mentioned conditions, one may get a required particle size, either a large or small one, with the simultaneous high conversion rate.

Additionally, it was found that in this case agglomeration phenomenon is in minority, and it does not affect the final particle size. However, the particle shape of CaF_2 crystals changes significantly with the change of Re number. The mentioned conditions of the precipitation processes may be very convenient in some cases connected with the product engineering, e.g., fine chemicals production.

In the investigated conditions, two independent fines producing sources have been recognized. One source is generated by the primary heterogeneous nucleation and has more than less constant rate when the second one is generated by attrition. The second source of nucleation strongly depends on the unit energy input (of mixing).

The crystal growth of CaF_2 particles is limited by means of the bulk diffusion.

The presented analysis of the destruction sources is consistent with the experimental data. The determination of a total energy destruction e_{tot} regardless of a mixer's type enables to anticipate the average crystal size. In the future, it is worth trying to put an effort and spread the proposed model to other solids obtained by precipitation together with considerations of some solid mechanical properties.

In the investigated conditions, the shear destruction energy does not play any role. The main causes of destruction are effective effects like crystal-crystal and crystal-inserts collisions, respectively.

Taking into consideration the power supply and the product yield only, one may distinguish the range of the Reynolds values in which the more profitable are static mixers and the range in which static mixers may be replaced by an empty pipe. For the Reynolds number greater than 1500, static mixers may be replaced by a pipe because the values of the CoV coefficient are almost the same and the attrition of solid is limited. The situation is reversed when Re numbers are lower than 1500. The efficiency of mixing (CoV value) is much better in a mixer than in an empty pipe, and the particle destruction in both cases is strongly reduced. It makes the static mixers like Koflo or Kenics a suitable tool for the realization of the precipitation process.

Nomenclature

$\mathrm{Re} = \rho \cdot w \cdot d/\eta'$:	Reynolds number
$Sc = \eta'/\rho \cdot D_{AB}$:	Schmidt number
A':	Constant in equations (7)–(9) (–)
a:	Ion activity (kmol/m^3)
B':	Constant in equation (8) (–)
B_0:	Nucleation rate (1/m^{3}s)
$B_{0_{prim}}$:	Primary nucleation rate (1/m^{3}s)
$B_{0_{second}}$:	Secondary nucleation rate (1/m^{3}s)
$\overline{C}$:	Mean concentration (kmol/m^3)
C_i:	Concentration in the ith sample
$C_{F^-_{init}}$:	Initial concentration of fluoride ions (kmol/m^3)
$C_{F^-_{fin}}$:	Final concentration of fluoride ions (kmol/m^3)
c:	Actual solution concentration (kmol/m^3)
c^*:	Solubility (kmol/m^3)
c_c:	Molar density of crystals (kmol/m^3)
c_{DC}:	Drag coefficient (–)
c_i:	Molar concentration of ion i (kmol/m^3)
Δc:	Supersaturation (kmol/m^3)
$\Delta c_{crit_{hom}}$:	Critical value of supersaturation for homogeneous nucleation (kmol/m^3)
D_{AB}:	Diffusivity (m^2/s)

d: Inner diameter of a device (m)
d_i: Diameter of the ith ion (m)
d_{mol}: Molecule diameter (m)
E_{coll}: Energy of mechanical collisions (J)
E_{shear}: Shear energy (J)
$E(t)$: Residence time distribution function (1/s)
e_{coll}: Unit energy of mechanical collisions (J/kg)
e_{shear}: Unit shear energy (J/kg)
e, e_{des}: Unit destruction energy (J/kg)
e_{eff}: Effective destruction energy (J/kg)
$e_{eff_{coll}}$: Effective energy of mechanical collisions (J/kg)
$e_{eff_{shear}}$: Effective shear energy (J/kg)
$e_{total_{SM}}$: Total unit energy in a static mixer (J/kg)
$e_{total_{pipe}}$: Total unit energy in the pipe (J/kg)
F: Cross-sectional area of a device (m^2)
f: Frequency of interactions (1/s)
h: Pitch of the static insert (m)
I: Ionic strength ($kmol/m^3$)
IP: Ionic product of activity ($(kmol/m^3)^3$)
K_{sp}: Solubility product ($(kmol/m^3)^3$)
k_v: Volume shape factor (−)
k_f: Surface shape factor (−)
L: Particle size (m)
L_m: Device length (m)
L_{mean}: Mean particle size (m)
L_i: Size of the ith crystal fraction (m)
$\Delta L_i = L_{i+1} - L_i$: Width of the ith grain class (m)
M: Molar mass (kg/kmol)
m_c: Crystal mass (kg)
n: Number of samples (−)
n_c: Number of crystals per unit volume ($1/m^3$)
n_0: Nuclei number density per unit volume ($1/m^4$)
$n(L)$: Population density ($1/m^4$)
Δp: Pressure drop (Pa)
Q_3: Particle undersize distribution (%)
q_3: Particle density distribution (1/m)
$S = \sigma + 1$: Supersaturation (−)
S': Standard deviation (−)
t^*: Temperature (°C)
t_m: Mean residence time (s)
$t_m max$: Maximum mean residence time (s)
u_r: Relative velocity (m/s)
$\dot{V}$: Volumetric flow rate (m^3/s)
V_c: Crystal volume (m^3)
V: Device volume (m^3)
V_{si}: Elemental volume within one static insert (m^3)
w: Fluid velocity (m/s)
w_i: Mass fraction of crystals (kg/kg)
z_i: Valence of the ith ion in a solution
α: Approach angle (°)
γ: Ion activity coefficient (−)
γ_{sl}: Interfacial tension (J/m^2)
δ_{av}: Averaged relative error (%)
ε: Energy dissipation rate (m^2/s^3)
η: Conversion rate (%)
η': Fluid dynamic viscosity coefficient (Pa·s)
ν: Fluid kinematic viscosity (m^2/s)
ρ: Fluid density (kg/m^3)
ρ_c: Crystal density (kg/m^3)
$\Delta\rho_c$: $\rho_c - \rho$ (kg/m^3)
σ: Relative supersaturation (−)
τ_{ind}: Induction time (s)
τ_{mic}: Micromixing time (s)
τ_s: Shear stresses (Pa)
φ: Volume fraction of crystals
υ: Sum of stoichiometric coefficients of reactants (−)
c: Crystal
c-c: Crystal–crystal
c-si: Crystal–static inserts
loc: Local value
CFD: Computational fluid dynamics
CoV: Coefficient of variation
CSD: Crystal size distribution
SEM: Scanning electron microscopy.

Data Availability

Previously reported pressure drop data were used to support this study and are available at 10.1002/cjce.22929. These prior studies (and datasets) are cited at relevant places within the text as reference [11]. Previously reported residence time distribution data were used to support this study and are available at 10.1002/cjce.22879. These prior studies (and datasets) are cited at relevant places within the text as reference [12]. Previously reported mixing homogeneity data were used to support this study and are available at 10.1002/cjce.23290. These prior studies (and datasets) are cited at relevant places within the text as reference [13].

Conflicts of Interest

The authors declare that they have no conflicts of interest.

References

[1] H. Møller and H. E. L. Madsen, "Growth kinetics of calcium fluoride in solution," *Journal of Crystal Growth*, vol. 71, no. 3, pp. 673–681, 1985.
[2] A. Mersmann and M. Kind, "Chemical engineering aspects of precipitation from solution," *Chemical Engineering and Technology-CET*, vol. 11, no. 1, pp. 264–276, 1988.
[3] K. Jiang, K. Zhou, Y. Yang, and H. Du, "A pilot-scale study of cryolite precipitation from high fluoride-containing wastewater in a reaction-separation integrated reactor," *Journal of Environmental Sciences*, vol. 25, no. 7, pp. 1331–1337, 2013.
[4] C. Y. Tai, M. J. Hon, and P.-C. Chen, "A comparison of growth behavior between $CaCO_3$ and CaF_2 crystals in a constant-composition environment," *Journal of the Taiwan Institute of Chemical Engineers*, vol. 42, no. 3, pp. 435–440, 2011.
[5] R. Aldaco, A. Garea, and A. Irabien, "Calcium fluoride recovery from fluoride wastewater in a fluidized bed reactor," *Water Research*, vol. 41, no. 4, pp. 810–818, 2007.

[6] A. J. Alvarez and A. S. Myerson, "Continuous plug flow crystallization of pharmaceutical compounds," *Crystal Growth and Design*, vol. 10, no. 5, pp. 2219–2228, 2010.

[7] T. Rivera and A. D. Randolph, "A model for the precipitation of pentaerythritol tetranitrate (PETN)," *Industrial and Engineering Chemistry Process Design and Development*, vol. 17, no. 2, pp. 182–188, 1978.

[8] M. Raphael, S. Rohani, and F. Sosulski, "Isoelectric precipitation of sunflower protein in a tubular precipitator," *The Canadian Journal of Chemical Engineering*, vol. 73, no. 4, pp. 470–483, 1995.

[9] Y. Dong, W. K. Ng, J. Hu, S. Shen, and R. B. H. Tan, "A continuous and highly effective static mixing process for antisolvent precipitation of nanoparticles of poorly water-soluble drugs," *International Journal of Pharmaceutics*, vol. 386, no. 1-2, pp. 256–261, 2010.

[10] Y. Dong, W. K. Ng, S. Shen, S. Kim, and R. B. H. Tan, "Solid lipid nanoparticles: continuous and potential large-scale nanoprecipitation production in static mixers," *Colloids and Surfaces B: Biointerfaces*, vol. 94, pp. 68–72, 2012.

[11] M. Stec and P. M. Synowiec, "Study of fluid dynamic conditions in the selected static mixers part I- research of pressure drop," *Canadian Journal of Chemical Engineering*, vol. 95, no. 11, pp. 2156–2167, 2017.

[12] M. Stec and P. M. Synowiec, "Study of fluid dynamic conditions in the selected static mixers part II-determination of the residence time distribution," *Canadian Journal of Chemical Engineering*, vol. 95, no. 12, pp. 2410–2422, 2017.

[13] M. Stec and P. M. Synowiec, "Study of fluid dynamic conditions in the selected static mixers part III–research of mixture homogeneity," *Canadian Journal of Chemical Engineering*, 2018, In press.

[14] M. Stec and P. M. Synowiec, "Investigation of CaF_2 precipitation in the selected static mixers," in *Proceedings of 20th International Symposium on Industrial Crystallization*, Dublin, Ireland, September 2017.

[15] T. Bayer, K. Himmler, and V. Hessel, "Don't be baffled by static mixers," *Chemical Engineering Journal*, vol. 5, pp. 50–57, 2003.

[16] R. Aldaco, A. Garea, and A. Irabien, "Particle growth kinetics of calcium fluoride in a fluidized bed reactor," *Chemical Engineering Science*, vol. 62, no. 11, pp. 2958–2966, 2007.

[17] C. Y. Tai, P. C. Chen, and T. M. Tsao, "Growth kinetics of CaF_2 in a pH-stat fluidized-bed crystallizer," *Journal of Crystal Growth*, vol. 290, no. 2, pp. 576–584, 2006.

[18] R. Aldaco, A. Irabien, and P. Luis, "Fluidized bed reactor for fluoride removal," *Chemical Engineering Journal*, vol. 107, no. 1–3, pp. 113–117, 2005.

[19] A. E. Nielsen and J. M. Toft, "Electrolyte crystal growth kinetics," *Journal of Crystal Growth*, vol. 67, no. 2, pp. 278–288, 1984.

[20] P. M. Synowiec, *Krystalizacja przemysłowa z roztworu*, WNT, Warszawa, Poland, 2008.

[21] A. Mersmann, B. Braun, and M. Löffelmann, "Prediction of crystallization coefficients of the population balance," *Chemical Engineering Science*, vol. 57, no. 20, pp. 4267–4275, 2002.

[22] P. Ayazi Shamlou, A. G. Jones, and K. Djamarani, "Hydrodynamics of secondary nucleation in suspension crystallization," *Chemical Engineering Science*, vol. 45, no. 5, pp. 1405–1416, 1990.

[23] P. Synowiec, A. G. Jones, and P. Ayazi Shamlou, "Crystal break-up in dilute turbulently agitated suspensions," *Chemical Engineering Science*, vol. 48, no. 20, pp. 3485–3495, 1993.

[24] E. P. K. Ottens and E. J. de Jong, "A model for secondary nucleation in a stirred vessel cooling crystallizer," *Kristall und Technik*, vol. 9, no. 8, pp. 873–886, 2006.

[25] A. Mersmann, *Crystallization Technology Handbook*, Marcel Dekker, New York, NY, USA, 2nd edition, 2001.

[26] A. E. Nielsen and O. Söhnel, "Interfacial tensions electrolyte crystal-aqueous solution, from nucleation data," *Journal of Crystal Growth*, vol. 11, no. 3, pp. 233–242, 1971.

[27] S. Deshpande and D. Kirwan, "Effect of mixing on size distribution during precipitation of L-aspargine in an agitated crystallizer," in *Proceedings of 14th International Symposium on Industrial Crystallization*, November 1999.

[28] R. Zauner, *Scale-up of precipitation processes*, Ph.D. thesis, University of London, London, UK, 1994.

[29] A. Mersmann, "Bei welcher Übersättigung soll man kristallisieren?," *Chemie Ingenieur Technik*, vol. 64, no. 11, pp. 991–999, 2004.

[30] J. Pohlisch and A. Mersmann, "The influence of stress and attrition on crystal size distribution," *Chemical Engineering & Technology-CET*, vol. 11, no. 1, pp. 40–49, 1988.

[31] P. Synowiec, "How to improve the crystal size distribution (CSD) in crystallizers with the inner suspension circulation," *Chemical Engineering and Processing: Process Intensification*, vol. 41, no. 7, pp. 585–593, 2002.

[32] R. K. Thakur, C. Vial, K. D. P. Nigam, E. B. Nauman, and G. Djelveh, "Static mixers in the process industries-a review," *Chemical Engineering Research and Design*, vol. 81, pp. 787–826, 2003.

[33] K. Inc., Koflo static in-line mixers, Tomorrow's technology, Today, Koflo Advertising Flyer, 1996.